

1   **Title**

2   **A corticostriatal deficit promotes temporal distortion of**  
3   **automatic action in ageing**  
4

5   **Author names and affiliations**

6   Miriam Matamales,<sup>1,2</sup> Zala Skrbis,<sup>1</sup> Matthew R. Bailey,<sup>3</sup> Peter D. Balsam,<sup>4</sup> Bernard W. Balleine,<sup>2</sup>  
7   Jürgen Götz,<sup>1</sup> and Jesus Bertran-Gonzalez<sup>1,2\*</sup>

8   <sup>1</sup>Clem Jones Centre for Ageing Dementia Research, Queensland Brain Institute, The University of  
9   Queensland, Brisbane, QLD, Australia

10   <sup>2</sup>Decision Neuroscience Laboratory, School of Psychology, University of New South Wales, Sydney,  
11   NSW, Australia

12   <sup>3</sup>Psychology Department, Columbia University, Broadway, NY, USA

13   <sup>4</sup>Psychology Department, Barnard College, Columbia University, Broadway, NY, USA  
14  
15

16   **\*For correspondence:** [j.bertran@unsw.edu.au](mailto:j.bertran@unsw.edu.au)  
17

## 18    **Abstract**

19    The acquisition of motor skills involves implementing action sequences that increase task efficiency  
20    while reducing cognitive loads. This learning capacity depends on specific cortico-basal ganglia  
21    circuits that are affected by normal ageing. Here, combining a series of novel behavioural tasks with  
22    extensive neuronal mapping and targeted cell manipulations in mice, we explored how ageing of  
23    cortico-basal ganglia networks alters the microstructure of action throughout sequence learning. We  
24    found that, after extended training, aged mice produced shorter actions and displayed squeezed  
25    automatic behaviours characterised by ultrafast oligomeric action chunks that correlated with deficient  
26    reorganisation of corticostriatal activity. Chemogenetic disruption of a striatal subcircuit in young mice  
27    reproduced age-related within-sequence features, and the introduction of an action-related feedback cue  
28    temporarily restored normal sequence structure in aged mice. Our results reveal static properties of  
29    aged cortico-basal ganglia networks that introduce temporal limits to action automaticity, something  
30    that can compromise procedural learning in ageing.



## 31 **Introduction**

32 Learning of new skills permits optimal interactions with the environment while reducing cognitive  
33 costs, a fundamental adaptation contributing to behavioural autonomy and automaticity in many  
34 species. Motor skills are generally implemented through sequence learning, which allows elementary  
35 action units to be integrated into behavioural streams (Lashley, 1951), reducing latency and increasing  
36 speed of action (Sternberg et al., 1978). Similar to memory, movement sequences are thought to be  
37 organised into “motor chunks”, a cognitive-motor strategy proposed to depend on cortico-basal ganglia  
38 circuitry (Graybiel, 1998; Wymbs et al., 2012) that allows expression of whole behavioural programs  
39 as a single response (Abrahamse et al., 2013).

40 Although initial learning capabilities are often preserved (Voelcker-Rehage, 2008; Matamales et  
41 al., 2016a), motor skill capacity is reduced in older adults, especially in tasks involving fine motor  
42 control. Indeed, some studies report that aged humans have a near zero capacity to form action chunks  
43 in newly acquired sequences (Shea et al., 2006; Verwey, 2010), whereas others find evidence of  
44 shortened motor chunks (Bo et al., 2009). Sequence learning appears, therefore, to be impaired in  
45 ageing, although the acquisition of new skills may still be possible, perhaps through the recruitment of  
46 compensatory strategies (Cabeza et al., 2002; Park and Reuter-Lorenz, 2009). Nevertheless, despite  
47 increasing knowledge of the neural bases of action automatisisation (Jin and Costa, 2015), the precise  
48 neuronal mechanism by which advanced ageing affects the acquisition of skills remains unknown.

49 To address this issue, we first designed behavioural tasks to determine which elements of action  
50 sequence learning were impaired by ageing. We then identified neuronal activation changes in the  
51 corticostriatal network that correlated with age-related learning defects, and reproduced some of these  
52 behavioural features through circuit-specific manipulations in young transgenic mice. Finally, we  
53 explored approaches to restore the ability of aged mice to perform action sequences through the  
54 introduction of an action-related feedback cue. Our findings suggest that the ageing brain may engage

particular neuronal strategies to automatise action during skill learning, and that environmental support in the form of action-related feedback can be used to correct this behaviour.

## Results

### Aged mice display shorter patterns of action

We first compared the ability of young (2 months old) and aged (20-22 months old) mice to develop action sequences. We focused on homogeneous sequences involving the concatenation of single responses because this procedure is particularly susceptible to chunking (Garcia-Colera and Semjen, 1987; Jin and Costa, 2015). After mild food restriction, we trained animals using an instrumental procedure in which the number of lever presses (LP) required to obtain food outcomes increased as training progressed on a random ratio schedule of reinforcement (from constant reinforcement, CRF, to random ratio 20, RR20; Figure 1A). The formation of action sequences was promoted by introducing a sequence trigger (ST), in which caching of 5 or 7 contiguous LP was required to access the current RR program (see Figure 1—figure supplement 1A). We used a novel approach to monitor the formation of sequences by parsing behavioural data into three elements: initiation (first LP, or LP occurring after a magazine check), execution (LP occurring after a LP) and termination (magazine check occurring after LP) (Figure 1B). Throughout training, both young and aged mice significantly escalated their overall performance (LP rate) as the ratio requirement to obtain an outcome increased (mixed ANOVA using factors of training and age  $F_{(3.5,48.9)} = 116.852$ ,  $p < 0.001$ ). A non-significant training x age interaction ( $F_{(3.5,48.9)} = 1.153$ ,  $p = 0.341$ ) suggested that overall instrumental performance was equal in young and aged mice (Figure 1—figure supplement 1B). However, half way through this training, aged mice produced a larger number of action sequences per minute, whereas young mice stabilised, or diminished, their sequence rates (Figure 1C). This was supported by a significant effect of training ( $F_{(16,224)} = 28.885$ ,  $p < 0.001$ ) and a significant training x age interaction ( $F_{(16,224)} = 3.716$ ,  $p < 0.001$ ).

Further, a comparison of action sequences between days 7 and 17 of training revealed that both young and aged mice were able to extend the number of execution elements in their sequences throughout training ( $F_{(1,14)} = 158.282$ ,  $p < 0.001$ ) (Figure 1D). This increase was of a different magnitude (as suggested by a significant day x age interaction ( $F_{(1,14)} = 40.03$ ,  $p < 0.001$ )), indicating that aged mice extended their sequences to a lesser extent than young mice. Separate analysis confirmed, however, that, although at a different level, both young ( $F_{(1,7)} = 108.562$ ,  $p < 0.001$ ) and aged ( $F_{(1,7)} = 106.664$ ,  $p < 0.001$ ) groups showed significant increases in sequence length (Figure 1D). In contrast, analysis of sequence duration showed a significant day x age interaction ( $F_{(1,14)} = 8.368$ ,  $p < 0.05$ ) with significant increases of sequence duration in young ( $F_{(1,7)} = 18.376$ ,  $p < 0.01$ ) but not aged ( $F_{(1,7)} = 1.745$ ,  $p = 0.228$ ) mice (Figure 1E). Importantly, aged mice showed evidence of learning about the ST applied from day 10, as they displayed a marked increase in the number of sequences that broke through the ST and therefore frequently accessed the RR schedule (Figure 1—figure supplement 1C). In contrast, young mice kept these numbers low, suggesting that they comfortably incorporated the ST requirement ( $F_{(3.065,42.908)} = 7.757$ ,  $p < 0.001$ ; training x age interaction  $F_{(3.065,42.908)} = 6.027$ ,  $p < 0.01$ ) (Figure 1—figure supplement 1C). Event-time plots recorded in both groups on day 7 revealed no sequence structure in their instrumental performance, despite all rewards being obtained by all of the mice (Figure 1—figure supplement 1D). In contrast, analysis on day 17 revealed that both young and aged mice developed clearly defined action sequences over time (with identifiable initiation, execution and termination elements), although these sequences were more frequent and much shorter in the aged group (Figure 1F).

We next ruled out that this effect was due to the inability of aged mice to hear when pellets were delivered (Figure 1—figure supplement 2). First, we confirmed that the delivery of pellets in the operant conditioning boxes generated a clear vibration signal, which was more salient than the sound of the dispenser engagement and/or pellet dropping (Figure 1—figure supplement 2A). We then exposed a group of young and aged mice to six days of magazine training, where 20 pellets were randomly

104 delivered in ~30 min sessions (Figure 1—figure supplement 2B-C). We found that all mice reduced  
105 their reaction time between pellet delivery and first magazine check (first check intervals) as training  
106 progressed (mixed ANOVA with factors training and age  $F_{(5,70)} = 25.822$ ,  $p < 0.001$ ), indicating that  
107 they learned to detect when pellets were delivered. A non-significant training x age interaction ( $F_{(5,70)} =$   
108  $0.360$ ,  $p = 0.874$ ) confirmed that this reduction was similar in both groups (Figure 1—figure  
109 supplement 2B and D). This similar performance was not due to a higher overall number of magazine  
110 checks in the aged group, since both young and aged mice showed a similar increase of magazine  
111 approach responses throughout this training ( $F_{(5,70)} = 25.822$ ,  $p < 0.001$ ; training x age interaction  $F_{(5,70)}$   
112  $= 0.360$ ,  $p = 0.874$ ) (Figure 1—figure supplement 2C). Overall, our results showed that aged mice  
113 produced a higher number of action sequences, and in contrast to previous studies in humans (Shea et  
114 al., 2006; Verwey, 2010), these sequences could be extended (in terms of action number) but not  
115 temporally sustained.

116 We thus explored whether sustained actions in aged mice were subject to temporal constraints,  
117 something that could explain the formation of shorter sequences of action. To address this, we used a  
118 Lever Hold (LH) instrumental procedure (Figure 2), a variant of the variable interval hold task (Bailey  
119 et al., 2015) in which the delivery of the reward depended on pseudorandom increments of LH time  
120 during training (Figure 2A & B). In this task, both young and aged groups displayed parallel  
121 escalations of LH times up to ~0.5 sec. However, young mice increased their LH times throughout  
122 subsequent stages of training, whereas aged mice maintained their maximum performance around 0.5  
123 sec holds (Figure 2C). Statistical analysis supported this observation: mixed ANOVA (factors: training  
124 and age) showed that the time of lever hold significantly varied as instrumental training progressed in  
125 both age groups ( $F_{(16,176)} = 73.471$ ,  $p < 0.001$ ), although there was a significant training x age  
126 interaction, indicating that the age of the animals significantly affected their performance ( $F_{(16,176)} =$   
127  $16.796$ ,  $p < 0.001$ ). Importantly, simple effects analyses confirmed that despite these differences, both  
128 groups independently elevated their performance throughout training (Young:  $F_{(16,112)} = 69.387$ ,  $p <$

0.001; Aged:  $F_{(16,64)} = 51.33$ ,  $p < 0.001$ ). Event scatter plots at different LH requirements revealed that, although both groups displayed a large number of very short presses, only young mice managed to produce sustained presses that approached, or exceeded, each LH requirement (Figure 2D). Event-time diagrams showed how all aged mice displayed much shorter holds than younger controls from the start of the session (Figure 2—figure supplement 1).

As such, these results provide evidence of action sequence formation in aged mice while also suggesting that these sequences could be influenced by temporal constraints, in line with previous results in humans (Bo et al., 2009).

### **Sequence learning leads to rapid response bursts and aberrant chunking in aged mice**

We next investigated the forms of automaticity generated in both age groups during LP-based sequence learning. First, we analysed in our sequence timestamp dataset whether aged mice showed higher overall sequence speed. We found that average speed on the last day of training was higher in aged mice, although the effect fell below significance ( $t_{(14)} = -2.104$ ,  $p = 0.054$ ) (Figure 3A). However, subsequent analysis of the serial response times based on inter-press-intervals (IPIs) recorded on the same day revealed that aged mice produced a much higher proportion of very short IPIs (Figure 3B, Figure 3—figure supplement 1A), suggesting that they were reaching a higher sequence speed than young mice. Due to a resolution limit in the timestamp data (Figure 3—figure supplement 1B), we sought to establish the true maximum sequence speed by means of acoustic data, where the fastest bursts of LP in each mouse were identified by extracting the acoustic fingerprint of lever depression (Figure 3C, see methods). We found a strikingly high speed of responding in aged mice, in some instances displaying spates of LP with over 13 presses per second, much faster than the fastest bursts recorded in young mice (Figure 3C, Video 1 and Video 2). These speeds are similar to fully automatised scratch reflex movements in mice (Inagaki et al., 2003). Quantification analysis of fast sequences confirmed that average speed within fast bursts (in number of presses/sec) was significantly

154 higher in aged than young mice ( $t_{(7.417)} = -4.201$ ,  $p < 0.01$ , Figure 3D), whereas within-burst IPIs were  
155 significantly shorter ( $t_{(14)} = 2.724$ ,  $p < 0.05$ , Figure 3E). Interestingly, despite their speed of responding,  
156 aged mice were less efficient at earning rewards ( $t_{(14)} = 3.101$ ,  $p < 0.01$ ), indicating that although their  
157 action bursts often broke through the sequence trigger (see Figure 1—figure supplement 1C), they  
158 rarely completed the RR requirements (Figure 3F).

159 We next sought to analyse whether different chunking patterns emerged in young and aged mice  
160 during sequence learning by studying the temporal relationships between consecutive action elements  
161 throughout training (Figure 3G-K). We categorised the action repertoire into two classes of interval: the  
162 within-sequence interval (IPIs that reside within each sequence) and the sequence boundary interval (a  
163 combination of press-check and check-press intervals that lay in-between sequences) (see methods).  
164 The analysis of the distribution of these intervals at different stages of training provided a visual  
165 readout of the chunking that emerged during sequence development (Figure 3G). In both young and  
166 aged mice, within-sequence IPIs (Figure 3G, blue) clustered around a similar interval space (from ~0.1  
167 to ~1 sec intervals) by day 13, suggesting that both groups developed chunking of within-sequence (i.e.  
168 execution) elements. In support of this, we found that both young and aged mice similarly reduced the  
169 within-sequence IPIs throughout training (Figure 3H), as reflected by a significant effect of training  
170 (two-way mixed ANOVA with factors training and age:  $F_{(1.955,27.377)} = 18.606$ ,  $p < 0.001$ ) but no  
171 training x age interaction ( $F_{(1.955,27.377)} = 0.562$ ,  $p = 0.573$ ). Similarly, the variability of these IPIs was  
172 equally reduced in both groups (Figure 3H, inset), again showing a significant effect of training  
173 ( $F_{(2.352,32.904)} = 6.545$ ,  $p = 0.003$ ) with no training x age interaction ( $F_{(2.352,32.904)} = 1.785$ ,  $p = 0.179$ ). On  
174 the other hand, the development of sequence boundary intervals throughout training (Figure 3G,  
175 orange) was very different in young and aged mice. Whereas young mice displayed longer boundary  
176 intervals that were distant from the chunking space, aged mice tended to accumulate them in a narrow  
177 band near the chunking space (Figure 3G). Importantly, this band appeared earlier in training (day 10)

178 in all aged animals, before within-sequence intervals chunked (Figure 3G, Figure 3—figure supplement  
 179 2A and B). This was evidenced in the quantitative analysis, where the young group showed an increase  
 180 in sequence boundary intervals from days 10 to 17, whereas the aged group kept these intervals  
 181 consistently low (Figure 3I), as indicated by a significant effect of training ( $F_{(3.884,54.375)} = 8.005$ ,  $p <$   
 182  $0.001$ ) and a significant training x age interaction ( $F_{(3.884,54.375)} = 4.729$ ,  $p = 0.003$ ). Although no drop in  
 183 variability for this interval was found from day 10 to 17 ( $F_{(7,98)} = 1.428$ ,  $p = 0.203$ ), aged mice  
 184 displayed lower variability than young mice in this period ( $F_{(1,14)} = 8.855$ ,  $p = 0.01$ ) (Figure 3I, inset),  
 185 suggesting that the temporal relationships of boundary elements in aged mice had already been  
 186 established in day 10 (see Figure 3—figure supplement 2). In order to obtain proportional measures of  
 187 chunking in both groups, we compared the within-sequence and sequence boundary intervals produced  
 188 by all young and all aged mice during the first 600 seconds of continuous action sequence behaviour  
 189 (Figure 3J-K). Again, we found in aged mice a larger proportion of very short within-sequence IPIs  
 190 (Figure 3J), although the overall number of within-sequence presses was equal across groups ( $t_{(14)} =$   
 191  $1.692$ ,  $p = 0.113$ ) (Figure 3J, inset). The sequence boundary intervals produced during this period were  
 192 also shorter in aged mice (Figure 3K), and the larger number of boundary elements in this group ( $t_{(7.341)}$   
 193  $= -4.248$ ,  $p = 0.003$ ) (Figure 3K, inset) reflected the higher number of action sequences produced by  
 194 aged mice per minute (see Figure 1C). Therefore, we found clearly different action automatization  
 195 processes shaping within-sequence and sequence boundary elements in young and aged mice. While  
 196 young mice appeared to exclusively chunk the elements within the sequences, aged mice displayed  
 197 ultrafast chunking of within-sequence elements, and showed evidence of early chunking in sequence  
 198 boundary elements. Together, these results suggest that early chunking of the extra sequence elements  
 199 in aged mice could cleave behaviour into ultrafast microchunks, revealing previously unrecognised  
 200 deficits in automatic action in ageing.

201

202 **Sequence features correlate with defective development of corticostriatal activity in aged mice**

203 The development of action sequences and stimulus-response habits is attributed to mediolateral shifts  
 204 of activity in cortico-basal ganglia circuits (Balleine, 2005; Yin et al., 2009; Balleine and O'Doherty,  
 205 2010), likely following a medial-to-lateral disposition of functionally relevant corticostriatal  
 206 projections in rodents (Hunnicutt et al., 2016; Voorn et al., 2004). Here, we studied the state of  
 207 activation of the corticostriatal network at different rostrocaudal levels in young and aged mice  
 208 expressing uninterrupted action sequences for 20 minutes (Figure 4). We identified over 60,000  
 209 activated neurons across cortical and striatal regions in sixteen mice using a confocal imaging-  
 210 computational approach based on the cyto-nuclear detection and mapping of phosphorylated MAPK  
 211 ERK1/2 (p-MAPK) (Figures 4A & B), a marker that is widely used to study neuronal activity  
 212 throughout the brain (Valjent et al., 2004). We first contrasted the extent of activation detected in  
 213 cortical and striatal regions in young and aged mice (Figure 4C). Two-way ANOVA (factors: age;  
 214 region) revealed no overall effect of age ( $F_{(1, 111)} = 1.868$ ,  $p = 0.174$ ), although there was a significant  
 215 age x region interaction ( $F_{(7,111)} = 2.136$ ,  $p < 0.05$ ). Simple effect analyses (factor: age) showed that this  
 216 interaction was primarily driven by differences in the anterior cingulate/motor area 2 (aCg/M2;  $F_{(1,14)} =$   
 217  $4.912$ ,  $p < 0.05$ ) and the frontoparietal regions of the cortex (FPx:  $F_{(1,14)} = 15.364$ ,  $p < 0.01$ ), as well as  
 218 in their target territories of the dorsolateral striatum (DLS:  $F_{(1,13)} = 4.753$ ,  $p < 0.05$ ) (Ebrahimi et al.,  
 219 1992; McGeorge and Faull, 1989). We next used this extensive dataset to identify the corticostriatal  
 220 regions that were primarily related to action sequence execution. We conducted a correlation study by  
 221 contrasting the corticostriatal activity profile based on p-MAPK activation in different cortical and  
 222 striatal areas in each mouse with the different features of sequence performance. We found that  
 223 sequence length, duration and speed of action displayed on the last day of training could only be  
 224 predicted by activation in DLS and FPx, whereas activation in all other areas did not significantly  
 225 correlate with any feature of sequence execution (Figure 4D). We then investigated the relative  
 226 functional engagement of different territories across the corticostriatal network in each age group by  
 227 performing a regional cross-correlation analysis in which the mean level of p-MAPK activation in each



228 region was correlated with all other regions across animals (Figure 4E). Young mice showed very low  
229 levels of correlation overall, with no significant relationships between cortical and striatal territories  
230 throughout the rostrocaudal extent of the network, perhaps due to automaticity-related reductions in  
231 neuronal variability and/or processing loads (Santos et al., 2015; Dayan and Daw, 2008) (Figure 4E,  
232 left panel). In contrast, aged mice showed widespread correlations that were significant in different  
233 regions of the corticostriatal network, especially the rostromedial, but not caudolateral, territories  
234 (Figure 4E, right panel). In order to obtain further regional information on this effect, we compared the  
235 spatial distribution of activated neurons in the corticostriatal network by mapping the position of  
236 individual neurons in each territory of sections from young and aged mice (Matamales et al., 2016b)  
237 (Figure 4F). Our data in aged mice revealed large regions within the DLS and deep layers of the FPx  
238 that were devoid of neuronal activation (Figure 4F). Overall, these results suggested an age-related  
239 deficit in the posterior corticostriatal network during action sequence execution that principally  
240 involved functional impairments in dorsolateral striatum and frontoparietal cortex, the two regions  
241 primarily implicated in motor chunking (Wymbs et al., 2012).

242

### 243 **Chemogenetic inhibition of direct pathway projection neurons in dorsolateral striatum increases** 244 **speed of action sequences**

245 Striatal output circuits are organised into direct and indirect pathway neurons (dSPNs and iSPNs,  
246 respectively), two parallel projection systems that orchestrate functions in the basal ganglia (Gerfen  
247 and Surmeier, 2011). Recent studies have suggested that action duration could be influenced by dSPNs  
248 in the DLS based on their sustained firing during the time of sequence execution (Jin et al., 2014), and  
249 the prolongation of an ongoing action by optogenetic stimulation (Tecuapetla et al., 2016). Capitalising  
250 on our p-MAPK mapping results, and based on findings that this intracellular activity marker is more  
251 sensitive in dSPNs than iSPNs (Bertran-Gonzalez et al., 2009), we hypothesised that age-related  
252 hypoactivation of dSPNs in the DLS could be contributing, at least in part, to deficits in action

sequence learning observed in aged mice. With the aim of reproducing the molecular deficit observed in DLS striatal neurons of aged mice throughout sequence learning, we used M4-based chemogenetics ( $G\alpha_i$ ) to prevent intracellular signalling in dSPNs of the DLS in young transgenic mice at the time of sequence implementation (i.e. day 10 onwards). *Drd1a*-Cre:*Drd2*-eGFP double transgenic mice were given a unilateral intra-DLS infusion of an AAV vector containing the  $G\alpha_i$ -hM4Di DREADD with Cre specificity coupled to the reporter mCherry, a procedure that allowed manipulation and visualisation of dSPNs and iSPNs, respectively (Figure 5—figure supplement 1). In order to test the validity of this system, we combined the injection of CNO (3 mg/kg, i.p.) with a delayed injection of GBR12783 (15 mg/kg, i.p.), a specific dopamine reuptake blocker known to induce p-MAPK in dSPNs (Valjent et al., 2010) (Figure 5—figure supplement 1B). We found that hM4Di-mCherry expression was contained, within the DLS, to eGFP-negative neurons, confirming specific infection of dSPNs in the DLS (Figure 5—figure supplement 1C, D). Importantly, dSPN-hM4Di expression and subsequent activation by CNO prevented GBR-induced MAPK phosphorylation when compared to the non-injected hemisphere of the same animals, ensuring that this system prevents intracellular activation (Figure 5—figure 1D). Quantification of p-MAPK<sup>+</sup> neurons confirmed this effect (Figure 5—figure supplement E): paired comparisons revealed a pronounced decrease of p-MAPK<sup>+</sup> neuron density ( $t_{(5)} = -15.565$ ,  $p < 0.001$ ) in equivalent areas of infected and noninfected hemispheres ( $t_{(5)} = -1.222$ ,  $p = 0.276$ ).

Based on the territories found to be devoid of p-MAPK<sup>+</sup> neurons in aged mice (see Figure 4F), we induced bilateral transduction of hM4Di DREADD into the DLS in a new cohort of young *Drd1a*-Cre<sup>+</sup>:*Drd2*-eGFP<sup>+</sup> (dSPN-hM4Di<sup>(+)</sup>) mice and their littermate controls (*Drd1a*-Cre<sup>-</sup>:*Drd2*-eGFP<sup>+</sup>; dSPN-hM4Di<sup>(-)</sup>) before LP sequence training (Figure 5A). From day 10 onwards, all mice received a 3 mg/kg CNO injection (i.p.) 45 min prior to the start of each session (Figure 5B). A two-way mixed ANOVA (factors: training; genotype) showed that the CNO treatment did not affect the ability of mice to acquire instrumental responses, as the rate of LP significantly increased as training progressed in both groups ( $F_{(16,192)} = 6.389$ ,  $p < 0.001$ ) (Figure 5—figure supplement 1F). Importantly, this treatment

278 did not cause a drop in overall performance (Figure 5—figure supplement 1F, compare days 9 and 10),  
279 which equivalently increased in both groups across training (training x genotype interaction:  $F_{(16,192)} =$   
280 0.601,  $p = 0.881$ ). This suggested that 3 mg/kg of systemic CNO did not cause detectable behavioural  
281 side effects.

282 We studied in these mice whether differences in sequence learning emerged throughout  
283 training, similar to the effects observed in aged mice (see Figure 1). We found that dSPN-hM4Di<sup>(-)</sup> and  
284 dSPN-hM4Di<sup>(+)</sup> mice produced a similar number of sequences per minute up to day 9, but hM4Di<sup>(+)</sup>  
285 littermates tended to display higher sequence rates once the CNO treatment started (Figure 5C), as  
286 supported by a significant between subjects effect in a two-way mixed ANOVA applied only on CNO  
287 days ( $F_{(1,12)} = 6.380$ ,  $p = 0.27$ ). Importantly, both groups showed an equal increase in the number of  
288 presses per sequence from day 10 (first day of CNO) to day 17 (Figure 5D). Accordingly, a two-way  
289 mixed ANOVA showed a significant increase in sequence length in all mice ( $F_{(1,12)} = 91.036$ ,  $p <$   
290 0.001), without a significant day x group interaction ( $F_{(1,14)} = 19.724$ ,  $p = 0.218$ ). This was further  
291 supported by simple effects (factor: day): both dSPN-hM4Di<sup>(-)</sup> and dSPN-hM4D<sup>(+)</sup> mice significantly  
292 increased their sequence lengths ( $F_{(1,6)} = 59.546$ ,  $p < 0.001$ ; and  $F_{(1,6)} = 33.521$ ,  $p < 0.01$ ; respectively),  
293 indicating that both groups were equally capable of extending (in terms of number of elements) their  
294 action sequences. In contrast, we found that only dSPN-hM4Di<sup>(-)</sup> controls increased the duration of  
295 their sequences from day 10 to 17, whereas dSPN-hM4Di<sup>(+)</sup> littermates displayed the same short  
296 latencies throughout (Figure 5E), as supported by a significant day x genotype interaction ( $F_{(1,12)} =$   
297 5.087,  $p < 0.05$ ). Simple effects confirmed a significant extension of action latency in dSPN-hM4Di<sup>(-)</sup>  
298 ( $F_{(1,6)} = 30.545$ ,  $p < 0.01$ ) but not dSPN-hM4Di<sup>(+)</sup> mice ( $F_{(1,7)} = 1.624$ ,  $p = 0.250$ ). Event-time plots  
299 recorded in both groups on day 17 revealed that both groups developed clearly defined action  
300 sequences (with identifiable initiation, execution and termination elements), although these sequences  
301 tended to be more frequent and shorter in dSPN-hM4Di<sup>(+)</sup> littermates (Figure 5—figure supplement  
302 2A-B).

303 We next sought to compare the patterns of action chunking displayed by both groups on  
 304 training day 18, similar to our previous study in young and aged mice (see Figure 3). We found that  
 305 dSPN-hM4Di<sup>(+)</sup> mice produced, overall, faster action sequences ( $t_{(12)} = -2.3841$ ,  $p = 0.035$ ) (Figure 5F),  
 306 and also displayed a higher proportion of short IPIs (Figure 5G). This was similar to the effect  
 307 observed in aged mice (see Figure 3A-B), although peak speeds within fast sequence bursts in dSPN-  
 308 hM4Di<sup>(+)</sup> were not as high as the ones recorded in aged mice. Temporal analysis of sequence elements  
 309 on day 18 revealed that dSPN-hM4Di<sup>(+)</sup> mice presented a shifted distribution of within-sequence  
 310 elements in the interval space (Figure 5H) and, consequently, displayed significantly shorter average  
 311 IPIs ( $t_{(12)} = 2.964$ ,  $p = 0.012$ ) (Figure 5J), which was a similar trend to that observed in aged mice (see  
 312 Figure 3J). However, we found no group differences in the distribution (Figure 5I) and average value  
 313 (Figure 3K) of sequence boundary intervals ( $t_{(12)} = 1.435$ ,  $p = 0.177$ ), which was in contrast to the  
 314 pattern observed in aged mice (see Figure 3K). Altogether, these findings suggest that interrupting  
 315 intracellular signalling in dSPNs of the DLS during periods of sequence development can increase the  
 316 speed of individual action sequences, although the number of elements fitted within each sequence as  
 317 well as the extra sequence intervals remained unaltered. Therefore, this manipulation reproduced  
 318 within-sequence but not extra-sequence features of action chunking in ageing, a pattern that could  
 319 explain the increased—rather than reduced—ability of dSPN-hM4Di<sup>(+)</sup> mice to obtain rewards during  
 320 ST training ( $t_{(12)} = -2.4$ ,  $p = 0.033$ ) (Figure 5L).

321

## 322 **Action-related feedback transitorily restores sequence structure in aged mice**

323 A possible source of the behavioural deficit we observed in aged mice is a loss of action-related  
 324 feedback; the use of environmental feedback in the form of action-associated cues has been reported to  
 325 improve self-initiated performance in older adults (Lindenberger and Mayr, 2014). We, therefore,  
 326 attempted to normalise the behavioural patterns of aged mice by providing action-related feedback in  
 327 the form of an external cue. We submitted two groups of aged mice to LP sequence training, both of

328 them receiving a sound cue (0.75 sec white noise) that signalled the last LP of each sequence preceding  
 329 the delivery of reward. For one of the groups the feedback cue was given for the duration of the  
 330 experiment (group Cue Maintained, days 1-36), whereas for the other group cue presentation stopped  
 331 on day 19 (group Cue Lost) (Figure 6A). This treatment had no apparent effects on the overall  
 332 performance of either group: two-way mixed ANOVA (factors: training; cue) showed that all mice  
 333 escalated their instrumental responses throughout the duration of the experiment ( $F_{(35,420)} = 72.869$ ,  
 334  $p < 0.001$ ), and there was no significant training x cue interaction ( $F_{(35,420)} = 1.378$ ,  $p = 0.078$ ) (Figure  
 335 6B). We then compared the sequence features displayed on days 7, 18 and 19, the latter being the first  
 336 day of cue withdrawal for the Cue Lost group (Figure 6C, D). Two-way mixed ANOVA (factors: day;  
 337 cue) showed significant differences in sequence length on days 7, 18 and 19 of training ( $F_{(2,26)} =$   
 338  $199.993$ ,  $p < 0.001$ ). However, there was a significant day x cue interaction ( $F_{(2,26)} = 6.567$ ,  $p < 0.01$ ),  
 339 suggesting that both groups performed differently across these days. Simple effects (factor: day)  
 340 confirmed that the sequence length dropped significantly from day 18 to day 19 in the Cue Lost group  
 341 ( $F_{(1,8)} = 15.696$ ,  $p < 0.01$ ), whereas it remained constant in the Cue Maintained group ( $F_{(1,5)} = 0.851$ ,  $p$   
 342  $= 0.399$ ) (Figure 6C). This effect was more pronounced on sequence duration: we found significant  
 343 differences in the duration of the sequences between days 7, 18 and 19 ( $F_{(2,26)} = 20.643$ ,  $p < 0.001$ ), and  
 344 again a significant day x cue interaction ( $F_{(2,26)} = 6.256$ ,  $p < 0.01$ ) with simple effects confirming that,  
 345 upon cue removal, the duration of action sequences dropped to pre-sequence levels in group Cue Lost  
 346 ( $F_{(1,8)} = 21.432$ ,  $p < 0.01$ ) but not in group Cue Maintained ( $F_{(1,5)} = 0.996$ ,  $p = 0.364$ ) (Figure 6D).  
 347 These results suggest that the execution of extended action sequences in aged mice depends on the  
 348 provision of action-related feedback instructing the duration of action.

349 We next investigated in these mice the transition from long to short sequences on cue  
 350 withdrawal (day 19). Event-time diagrams representing the sequences executed at the beginning and at  
 351 the end of the training session showed that all mice in group Cue Lost started by executing long action  
 352 sequences even in the absence of the auditory cue, but that these sequences rapidly shortened

353 throughout the session (Figure 6E, F; Figure 6—figure supplement 1A, B). Accordingly, two-way  
354 mixed ANOVA (factors: sequence number; period) showed overall significant differences in the length  
355 of the sequences as the session progressed ( $F_{(9,144)} = 3.635$ ,  $p < 0.001$ ). However, there was a  
356 significant sequence number x period interaction ( $F_{(9,144)} = 218,993$ ,  $p < 0.01$ ), indicating that the  
357 length was significantly different in the Start and End periods of the session. Simple effects analysis  
358 (factor: sequence number) revealed that the length of the sequences progressively decreased at the start  
359 of the session ( $F_{(9,72)} = 5.089$ ,  $p < 0.001$ ), but remained constant towards the end ( $F_{(9,72)} = 0.921$ ,  $p =$   
360  $0.512$ ) (Figure 6F). Importantly, the shortening of action sequences precipitated by cue removal was  
361 translated into a dramatic increase in the total number of sequences expressed by the Cue Lost mice  
362 that persisted throughout training (Figure 6G), as indicated by a significant day x cue interaction  
363 ( $F_{(35,420)} = 2.339$ ,  $p < 0.001$ ).

364 Finally, we assessed the action chunking patterns across training in both groups of aged mice and how  
365 these patterns changed with cue removal (Figure 6H). We found that, despite the presence of the  
366 feedback cue, both groups of mice displayed similarly aberrant automaticity on day 10, with boundary  
367 intervals accumulating in a narrow band nearby the chunking space (Figure 6H, day 10). However,  
368 mice seemed to learn to categorise their sequence elements with further cued training as the boundary  
369 interval band disappeared in both groups (Figure 6H, Day 18). Strikingly, group Cue Lost precipitated  
370 microchunks as soon as the instructive cue was removed (Figure 6H, compare days 18 and 22). Taken  
371 together, these results show that aged mice can execute longer action sequences as long as action-  
372 related feedback is provided regarding sequence duration, suggesting that this deficit is cognitive-motor  
373 rather than purely executional in origin.

374

## 375 Discussion

376 In the present study, we combined a series behavioural designs with comprehensive neuronal mapping  
377 and targeted circuit manipulation to reveal a fundamental deficit in the development of action  
378 sequences in mice of advanced age (20-22 m.o., average life expectancy is 24 months). It is well  
379 known that certain forms of motor skill learning are impaired in older adults (Voelcker-Rehage, 2008).  
380 In procedural learning, studies in humans demonstrate that both early (65-68) and late elderly (75-88)  
381 show very limited use of motor chunking during multi-element sequence tasks (Shea et al., 2006;  
382 Verwey, 2010). Although the precise patterns of action chunking differ between homogenous and  
383 heterogeneous sequence learning (i.e. sequences involving one vs. more than one action element)  
384 (Garcia-Colera and Semjen, 1987; Sternberg et al., 1978), our results in mice pressing a single lever  
385 revealed that older subjects consistently developed a form of chunking that involved shorter and faster  
386 sequences (microchunks, see Video 2). Similarly, using a serial response time task in humans, in which  
387 the formation of chunks was encouraged using visuospatial cues, Bo et al. (2009) found that older  
388 adults developed motor chunks overall, although the length of those chunks was reduced. Taken  
389 together, these results suggest that the automation of actions is possible in the aged, but is temporally  
390 distorted compared to that expressed by younger individuals.

391 Over and above the task-efficiency benefits of well-developed skills, automated or model-free  
392 behaviour has advantages for computational and space complexity loads; operationally, model-free  
393 reinforcement learning systems require less memory than model-based systems (Schneider and  
394 Shiffrin, 1977; Dayan and Daw, 2008). One important implication of this is that implementing model-  
395 free operations is more appropriate when computational resources such as working memory are limited  
396 (Otto et al., 2013). On this account, the computational resources of the aged brain can be limited by its  
397 clearly reduced working memory capacity (Bo et al., 2009; Wang et al., 2011; Wingfield et al., 1988).  
398 Therefore, in light of these memory caching limits, implementing model-free or automatic processes  
399 early in training can be seen as a successful strategy. Although this perspective can tentatively explain

400 the formation of premature, unbreakable microchunks during early stages of training in aged mice,  
401 there are two features of our data that could argue against it. First, model-based to model-free transition  
402 (i.e., goal-directed to habitual modes of action) is thought to rely on shifts from dorsomedial to  
403 dorsolateral corticostriatal networks (Balleine, 2005; Yin et al., 2009). In the particular case of  
404 sequence learning and action chunking, engagements of posterolateral corticostriatal circuits have been  
405 demonstrated in humans and animals that are producing clearly automatised instrumental behaviours.  
406 Wymbs et al. (2012) found in humans that activity in the frontoparietal cortex and sensorimotor  
407 putamen (equivalent to the posterior dorsolateral striatum in rodents) strongly predicts critical features  
408 of action sequence execution, and studies in mice have provided information on the specific circuitry  
409 within posterior dorsolateral areas involved in action sequence initiation, execution and termination  
410 (Jin and Costa, 2010; Jin et al., 2014; Tecuapetla et al., 2016). Accordingly, a premature  
411 implementation of model-free processing (such as observed in microchunking) should predict an early  
412 medio-lateral shift of activity in corticostriatal networks. However, our neuronal activity assessments in  
413 aged mice suggest the contrary: aged brains seem to fail to disengage rostro-medial corticostriatal  
414 circuits, and shorter and faster sequences predict lower activity in dorsolateral regions of the striatum  
415 (Figure 4). Similarly, preventing such a shift in young mice by disrupting the activity of a subset of  
416 neurons in the dorsolateral striatum early in training reproduced some aspects of the aged behaviour,  
417 including the shorter latencies and higher speeds (see Figure 5).

418 Secondly, the formation of premature microchunks is not consistent with the results of our last  
419 experiment, where similar oligomeric sequences were instantly precipitated by the loss of an action-  
420 related feedback cue (Figure 6). In this case, aged mice expressed long, uninterrupted sequences from  
421 the beginning of training, and never displayed the constricted sequences prior to the loss of the cue.  
422 These results suggest that the execution of microchunks is not a consequence of deficient learning, but  
423 rather the result of different automaticity processes put in place by the aged brain.



424        Rather, our study supports the notion that young and aged brains start from a different neuronal  
425        environment or scaffolding (Park and Reuter-Lorenz, 2009), and attempt to optimise instrumental task  
426        performance by implementing entirely different strategies for automaticity. The critical question is:  
427        what are the features of the aged brain that produce these shorter patterns of action? Our data suggest  
428        that the dynamic medial-to-lateral shifts that are predicted to occur in the corticostriatal network during  
429        the development of automatic behaviour (Yin et al., 2009) may not happen, or may only occur  
430        partially, and this neuronal staticity might be key to explaining the recruitment of unusual automaticity  
431        processes in aged mice. Indeed, several functional imaging studies in humans suggest a similar shift in  
432        activity to anterior regions of the brain in elderly subjects (see Park and Reuter-Lorenz, 2009 for an  
433        extensive review): a compensatory overactivation in declining prefrontal cortical regions drives the use  
434        of different behavioural strategies to those of younger adults in certain tasks (Cabeza et al., 2002;  
435        Gutchess et al., 2005; Raz, 2005). This can be regarded as one possible mechanism for the marked  
436        differences in motor chunk development in aged humans during sequence learning (Bo et al., 2009;  
437        Verwey, 2010; Wymbs et al., 2012).

438        Nevertheless, why an anterior shift in corticostriatal activity with ageing generates such  
439        constricted spurts of action during sequence execution remains unresolved. Again capitalising on age-  
440        related working memory deficits and prefrontal cortex dysfunction (Wang et al., 2011; Wingfield et al.,  
441        1988), one could speculate that the overactivity observed in prefrontal areas in aged individuals reflects  
442        failed attempts to boost working memory capacity in distal parietal cortical regions, following a similar  
443        process to that proposed in computational models of visuospatial working memory retention (Edin et  
444        al., 2009). Interestingly, our data reveals specific activation reductions in dorsomedial prefrontal cortex  
445        as well as frontoparietal cortex, regions likely to be part of the prefronto-parietal network for top-down  
446        control of working memory capacity (Edin et al., 2009; Gruber and Goschke, 2004). Certainly, these  
447        prefrontal deficits could contribute to part of the problem, although the question of how working

448 memory contributes to action organisation remains largely unresolved and is complex, likely involving  
449 subcortical basal ganglia circuitry (O'Reilly and Frank, 2006).

450 Another, perhaps related, neuronal process that could in part explain the microchunk behaviour in  
451 our study is malfunction in the prefronto-basal ganglia network and related deficits in temporal control  
452 with ageing (Gunstad et al., 2006). One interesting possibility is that the aged brain is subject to  
453 constraints during the temporal scaling of sequence processing in corticostriatal networks (Fukai, 1999;  
454 Igarashi et al., 2013). Although the precise mechanism by which time is encoded in the brain is  
455 unknown, recent evidence clearly implicates subcortical networks (dorsal striatum) as a key structure in  
456 scaling time for action (Mello et al., 2015; Soares et al., 2016). In our study, we found that selectively  
457 reducing the activity of direct pathway spiny projection neurons (dSPNs) in dorsolateral regions of the  
458 striatum reduced action duration while increasing action speed. These results directly support and  
459 extend recent findings on the involvement of dSPNs in encoding of the latency of action. Jin et al.  
460 (2014) found that a large proportion of dSPNs recorded in the dorsolateral striatum showed sustained  
461 patterns of firing that spanned the duration of an action sequence. More recently, the same group found  
462 that optogenetic stimulation of these neurons in the same striatal territory extended the length and  
463 duration of ongoing action sequences only during periods of stimulation (Tecuapetla et al., 2016). It  
464 should be emphasised, however, that although our striatal manipulations may have recapitulated some  
465 of the microchunking features observed in aged mice, we did not attempt to recreate accompanying  
466 prefronto-parietal dysfunction (and the resulting working memory deficit). This might explain why our  
467 young mice with the striatal manipulation were still capable of building up a reasonable action  
468 structure, something that unexpectedly rendered the animals more efficient at obtaining outcomes  
469 (Figure 5). Thus, our results add to studies elucidating the microcircuitry responsible for the temporal  
470 scaling of action, and suggest the intriguing possibility that the static properties of aged cortico-basal

471 ganglia networks have direct effects on the duration of action sequences, compromising behavioural  
472 automaticity.

473       In conclusion, we provide evidence for a severe deficit in corticostriatal function during normal  
474 ageing in mice that engenders a distortion of action sequences after extended training. Our findings  
475 have implications for skill learning in ageing and point to the stationarity of cortico-basal ganglia  
476 transmission as a major feature of the aged brain hampering its ability to acquire new skills.  
477 Importantly, we found that action-related feedback cues given throughout training transitorily solves  
478 this problem, a solution that could be readily implemented in current rehabilitation strategies and  
479 behavioural therapies for cognitive ageing (Lindenberger and Mayr, 2014).

## 480 **Materials and Methods**

### 481 **Mice**

482 All procedures were approved by the University of Queensland Animal Ethics Committee  
483 (QBI/412/14/NHMRC and QBI/027/12/NHMRC) in accordance with the *Animal Care and Protection*  
484 *Regulation* (Queensland Government, 2012) and the *Australian Code of Practice for the Care and Use*  
485 *of Animals for Scientific Purposes* (National Health and Medical Research Council, 2013).

486 C57BL6/J mice (RRID:IMSR\_JAX:000664) were purchased from the Animal Resources Centre  
487 (Perth, Australia), and an ageing colony was established in the Queensland Brain Institute Animal  
488 Facility. Young mice used for the experiments were 2 months old at the beginning of the experiments,  
489 whereas aged mice were 20-22 months old. Transgenic mice were purchased from the Mutant Mouse  
490 Resource & Research Centers (MMRRC, NIH) and outbred to C57BL6/J (RRID:IMSR\_JAX:000664)  
491 for more than 6 generations in the Queensland Brain Institute Animal Facility. Heterozygous *Drd1a-*  
492 *Cre*<sup>+/-</sup> mice (strain B6(Cg)-Tg(Drd1a-cre)FK150Gsat/Mmucd [RRID:MMRRC\_029178-UCD]:  
493 expresses Cre in dSPNs) were bred with homozygous *Drd2*-EGFP mice (strain B6(Cg)-Tg(Drd2-  
494 EGFP)S118Gsat/KreMmucd [RRID:MMRRC\_036931-UCD]: expresses EGFP in iSPNs). This  
495 crossing produced 50% of *Drd1a*-Cre<sup>+/-</sup> *Drd2*-eGFP<sup>+/-</sup> mice and 50% of *Drd1a*-Cre<sup>-/-</sup> *Drd2*-eGFP<sup>+/-</sup>  
496 mice, which were used in the experiments at 2 months of age. All mice weighted 23-26 g (young) and  
497 28-34 g (aged) at the beginning of each experiment, although food intake was restricted throughout  
498 most of the experiments (mice were maintained at approximately 85% of their free-feeding weight). All  
499 mice were housed in plastic home cages (Optimice, Animal Care Systems, CO) in a climate-controlled  
500 colony room on a 12-h light/dark cycle and handled daily, and were allowed *ad libitum* access to water.  
501 Littermates in each home cage were maintained throughout the experiment, and were randomly  
502 allocated to each experimental group.

503

504

505 **Behavioural procedures**

506 *Apparatus.* All training procedures were carried out in sound- and light-resistant operant chambers  
507 (MED Associates, PO). The chambers were illuminated with a 3 W, 24 V house light. Each chamber  
508 contained a recessed feeding magazine in the center of the right side wall connected to two individual  
509 food dispensers that could deliver 20 mg dustless precision pellets (Bio Serv, NJ, #F0163) into the  
510 magazine when activated. Either side of the magazine contained retractable levers. Med-PC software  
511 was used to direct the insertion and retraction of the levers, illumination of the light and delivery of the  
512 pellets. The software allowed the recording of timestamp events each 10 msec, including the number of  
513 lever presses, magazine entries and food pellets delivered throughout the duration of the experiment.  
514 Activity was also monitored using D-Link DCS-932L IP LED infrared cameras (VGA 1/5 inch CMOS  
515 sensor with built-in microphone) through D-ViewCam Software (D-link Corporation, Taiwan).

516

517 *Magazine training.* Prior to all instrumental procedures, mice were exposed to four or six days of  
518 magazine training in the operant chambers (1 session/day). Each mouse was assigned one operant  
519 chamber, which was maintained throughout the duration of the experiment. The chamber light was  
520 illuminated to signal the beginning of the session and extinguished at its termination. Both levers were  
521 retracted and mice explored the chamber freely. Twenty grain food pellets (20 mg, 3.35 kcal/g each)  
522 were delivered into the magazine at random time intervals (RT 60 seconds) over ~30 min. These pellets  
523 differed in taste but were calorically similar (grain: 3.35 kcal/g, purified: 3.6 kcal/g). Consumption of  
524 pellets was monitored at the end of each session.

525

526 *Standard instrumental training.* All behavioural procedures were based on single-lever operant  
527 conditioning and started with a standard instrumental training module. Each training session began  
528 with the illumination of the chamber light and insertion of the two levers into the operant box, and

ended with the extinguishing of the chamber light and lever retraction. The mice were exposed to one training session each day where only one of the levers was contingent to the delivery of the pellets (active lever). Assignment of right or left active lever was counterbalanced across mice. Each training session continued until mice had received a total of 20 pellets, or the session timed out at 30 min. For the first three days of instrumental training (days 1-3), mice were trained on a constant reinforcement schedule (CRF); every lever pressing action was rewarded. The probability of the outcome given a response (P) was gradually shifted over the following days of training using increasing random ratio (RR) schedules of reinforcement: a RR5 schedule ( $P = 0.2$ ) was always used on days 4–6, and RR10 ( $P = 0.1$ ) and RR20 ( $P = 0.05$ ) were applied from day 7 as indicated in each particular experiment (see below).

**Sequence training.** Sequence training procedures started with standard instrumental training (days 1-6). RR10 and RR20 were then applied as indicated in each experiment (see Figures 1A, 5E and 6A). In parallel to this schedule of reinforcement, an additional rule to promote sequence learning was applied from day 10 onwards (sequence trigger, ST, Figure 1—figure supplement 1), which limited the access to RR reinforcement to action sequences that were initiated with at least 5 (applied from day 10) or 7 (applied from day 13) consecutive lever presses. Sequences that were truncated with a termination element (lever press → magazine entry) before reaching the fifth or seventh consecutive press blocked access to the RR program. Unlocked sequences ( $\geq 5$  initial presses) that were truncated with a termination element before earning reward also reset the RR trial. This was achieved in MED PC-IV by caching and verifying, for each lever press, the identity of the behavioural elements stamped 5 or 7 positions back in the timestamp array along each round of reinforcement. On training day 18, the mice underwent an additional training session that lasted for 20 minutes and had no limit of rewards prior to perfusion (see section “Transcardial fixation and tissue sectioning” below). In the feedback cue experiment (Figure 6), the termination element in each sequence (i.e., the lever press that triggered the

554 delivery of the reward) was cued with a 0.75s white noise throughout training (see Figure 6A). On day  
555 19, the cohort of mice was divided in two groups, according to matching performances. Group  
556 Maintained kept the same procedure with cued sequences until day 36, whereas Group Lost stopped  
557 receiving such cue but kept all the other parameters of the task unchanged. Mice in Group Lost were  
558 run in a separate session to prevent sound propagation from cued animals.

559

560 **LH training.** Lever Hold (LH) operant conditioning procedures (Figure 2) were a variation of our  
561 previously reported variable interval hold task (Bailey et al., 2015), and started with standard  
562 instrumental training (days 1-3), where each individual press was reinforced (CRF or LH0). The  
563 probability of outcome delivery was then rendered dependent on the time of lever hold, and was  
564 gradually shifted over the following days of training using increasing pseudorandom lever hold  
565 (LH0.3-LH5) intervals. During LH0.3 (days 4-6), the distributions of required hold durations had a  
566 mean of ~0.3 s (LH0.3: min = 0.05 sec; max = 0.88 sec). The required hold durations for the  
567 subsequent sessions were drawn from an exponential distribution with a higher mean (LH0.8 [days 7-  
568 9], LH2 [days 10-12], LH3.2 [days 13-15] and LH5 [days 16-17]). Thus, during the final session of LH  
569 training, subjects were required to hold down the lever for intervals that averaged 5 sec but could be as  
570 long as 11.7 sec.

571

## 572 **Chemogenetics**

573 Specific inhibition of dSPNs regionally contained in the DLS was achieved by pulse-based  
574 microinjection of Cre-dependent hM4Di DREADDs virus (AAV2-hSyn-DIO-hM4D(Gi)-mCherry,  
575 UNC Vector Core, NC) into the DLS at two different rostro-caudal levels of *Drd1a*-Cre<sup>+/-</sup> *Drd2*-  
576 EGFP<sup>+/-</sup> and *Drd1a*-Cre<sup>-/-</sup> *Drd2*-EGFP<sup>+/-</sup> double transgenic mice through stereotaxic surgery  
577 (coordinates: R-C: +1.1/+0 mm [bregma]; M-L: ±2/±2.75 mm [bregma]; D-V: -2.625/-2.75 mm [skull  
578 surface]) combined with an intraperitoneal injection of clozapine N-oxyde (CNO; dissolved in saline to

3 mg/kg; NIMH Chemical Synthesis and Drug Supply Program, Bethesda, MD). In order to validate the effects of this manipulation, a first cohort of these mice (2 *Drd1a*-Cre<sup>-/+</sup> *Drd2*-EGFP<sup>+/-</sup> and 2 *Drd1a*-Cre<sup>-/-</sup> *Drd2*-EGFP<sup>+/-</sup>) was used where the virus was injected unilaterally (see Figure 5A). After recovery from surgery, these mice received a first injection of CNO and 30 minutes later another injection of GBR12783 (15 mg/kg, i.p. dissolved in sterile water) prior to rapid intracardial perfusion (see Figure 5A-C). Animals used for sequence training received a bilateral injection of the virus and were injected with CNO on days 10-17 45 min prior to the start of the training session (see Figure 5D-L).

### **Stereotaxic surgery**

Mice were pre-anesthetised in an induction chamber with oxygen/isoflurane mixture (Laser Animal Health, Pharmachem, Australia). Pedal reflex was used to monitor anesthesia before placing the mouse in the stereotaxic frame (Kopf Instruments) fitted with a mask supplying a continuous flow of oxygen/isoflurane mixture (1L/min oxygen, 1.5 ml/min isoflurane). Once deeply anesthetised, a 1.5 cm incision was made to expose the skull. For each microinjection, a small hole was pierced (~0.2 mm width) at the appropriate A-P and M-L coordinates (see above). A pulled glass capillary (GC100TF-15, Harvard Apparatus) was pulled using a micropipette puller (P-97, Sutter Instrument) and pre-filled with the solution and fitted into a Nanoject II (Drummond Scientific) before being slowly inserted vertically through each hole until reaching target (D-V coordinate). Once in target, injections were preceded by a 2-min waiting interval. Two sets of pulse injections of hM4Di-DREADDs AAV were delivered in one (unilateral experiments) or both (bilateral experiments) sides of the brain. Each injection consisted of 14 pulses of 69 nL spaced by 30 sec. Two min after the last pulse, the pipette was gently pulled out, and the incision was closed with surgery suture silk and sealed with tissue adhesive (3M Vetbond). Animals were placed in cages separately on a warming plate (37°C) during recovery. A pre-operative s.c. administration of butorphanol (torbugesic, 3mg/kg) ensured analgesia during and after the



604 intervention. The antibiotic Baytril (5mg/Kg) was administered at the end of the procedure. Both  
605 torbugesic and baytril were administered once a day for 2 days after surgery. Behavioural procedures  
606 started after a 3-week recovery period. None of the mice displayed perceptible wounds by the start of  
607 the behavioural experiments.

608

## 609 **Tissue processing and immunofluorescence**

610 ***Transcardial fixation and tissue sectioning.*** Twenty min after the start of the session (day 18), the  
611 mice were rapidly anesthetised by exposure to 10 sec of isoflurane gas (4% in air; Laser Animal  
612 Health, Pharmachem, Australia) in a sealed chamber, followed by a lethal intraperitoneal injection of  
613 sodium pentobarbital (500 mg/kg; Virbac Pty. Ltd., Australia). After ensuring deep anesthesia by  
614 testing paw and tail reflexes, mice were perfused transcardially using an air pressure system (constant  
615 flow of 15 ml/min) with 4% paraformaldehyde (PFA) in a solution of 0.1 M sodium phosphate buffer  
616 (pH 7.4). Brains were dissected and post-fixed overnight in PFA solution at 4°C. Consecutive 30 µm  
617 coronal sections spanning the rostro-caudal extent of the striatum were obtained for each animal using  
618 a vibratome (VT1000s, Leica Microsystems, Germany). Free-floating slices were stored at -20°C in a  
619 cryoprotectant solution (30% ethylene glycol, 30% glycerol, 0.1 M sodium phosphate buffer) until  
620 processed for immunofluorescence.

621

622 ***Immunofluorescence.*** Free-floating slices were rinsed 3 times in Tris-buffered saline (with sodium  
623 fluoride id phosphorylations were detected: TBS NaF; 0.25 M Tris, 0.5 M NaCl, 0.1 mM NaF, pH 7.5)  
624 for 10 min on an orbital shaker at room temperature prior to membrane permeabilisation treatment  
625 (0.3% triton X-100 in TBS [NaF]), which was applied for 1 h. After three 10-min washes with TBS  
626 (NaF), slices were incubated at 4°C on an orbital shaker with a rabbit polyclonal anti- threonine 202  
627 and tyrosine 204-phosphorylated p44/42 MAPK-ERK1/2 primary antibody (p-MAPK; diluted 1:500;  
628 Cell Signaling Technology, MA; Cat# 9101L RRID:AB\_331647). Following a 24-h incubation period,

unbound primary antibodies were washed off with 3 washes of TBS (NaF), and bound primary antibodies were detected through incubation for 1 h at room temperature with donkey anti-rabbit fluorescent Cy3-conjugated secondary antibodies (diluted 1:800, Jackson ImmunoResearch Laboratories, PA). In the viral infection studies, simultaneous detection of iSPN fluorescence (*Drd2*-eGFP), dSPN virus expression (*Drd1a*-hM4Di-mCherry) and neuronal activation (p-MAPK, Cy5 donkey anti-rabbit antibody, 1:800 dilution) was conducted. Unbound secondary antibodies were washed off through 4 final rinses in TBS. Samples were then placed on Superfrost Plus coated slides (Thermo Fisher Scientific, MA) and mounted with a coverslip on Vectashield fluorescence medium with or without DAPI nuclear staining (Vector Laboratories, CA). Slides were stored at 4°C in the dark until image acquisition.

639

#### 640 **Image acquisition**

All image datasets in this study were obtained in the Queensland Brain Institute Advanced Microimaging and Analysis Facility.

643

**Spinning disk microscopy.** Neuronal activity mapping experiments were performed through wide-field spinning disk confocal microscopy. A spinning disk confocal microscope (W1 Yokogawa spinning disk module; Zeiss Axio Observer Z1) equipped with sCMOS camera (Hamamatsu Flash 4.0 with 2048 x 2048 chip) was used to capture p-MAPK-labeled individual tiles (optical magnification: 20X; pixel depth: 16 bit; image resolution: 0.625 pixels/μm; image size: 1024 x 1024 pixels, 561 laser). Tiles were stitched together using Slidebook 6.0 software to reconstruct a high-resolution image of bilateral striata. In each mouse, 3 sections at the following approximate coordinates were reconstructed (A-P distance from bregma): 1.7 mm (rostral, 1.1 mm (medial) and 0.15 mm (caudal). Three-channel tiles (488 nm, 561 nm and 637 nm lasers) were obtained in viral infection experiments.

653

654 **Scanning confocal microscopy.** Simultaneous analysis of iSPN eGFP fluorescence, hM4Di-mCherry  
655 virus expression and p-MAPK distribution was performed through point scanning confocal  
656 microscopy. Single plane confocal images (optical magnification: 40X; averaging scans: 4; pixel depth:  
657 12-bit) were captured using a Zeiss LSM 710 confocal laser-scanning microscope (Carl Zeiss AG,  
658 Oberkochen, Germany). Three-channel images (488 nm, 561 nm and 633 nm lasers) of the dorsolateral  
659 striatum were taken for each hemisphere in 2 *Drd1a*-Cre<sup>-/+</sup> *Drd2*-EGFP<sup>+/-</sup> and 2 *Drd1a*-Cre<sup>-/-</sup> *Drd2*-  
660 EGFP<sup>+/-</sup> mice.

661

## 662 **Data acquisition and analysis**

663 **Action data (timestamp).** [Figure 1-source data 1, Figure 2-source data 1, Figure 5-source data 1,  
664 Figure 6-source data 1, Figure 1-source data 3] A combination of MEDState Notation (MSN, MED  
665 Associates) language and a series of customised MATLAB (MathWorks, Natick, MA) scripts were  
666 used to retrieve, sort and plot timestamp datasets. All individual events (left and right lever press,  
667 magazine entries, and pellet deliveries) that occurred during each training session were recorded. The  
668 time at which each event occurred (y matrix) was stamped with a 10 ms resolution (z matrix,  
669 centiseconds). On each subject, streams of timestamp data of each category (i.e. 1-4) were combined  
670 and chronologically organised. Discrete sequences and their initiation, execution and termination  
671 elements were then identified based on the interspacing of lever presses and magazine checks.  
672 Consecutive magazine checks produced after the termination of a sequence were ignored. Parameters  
673 such as within-sequence inter-press-intervals (IPIs), sequence length (number of actions per sequence)  
674 and sequence latency (time elapsed from initiation to termination) were calculated at this point for each  
675 sequence, and average values were obtained for each mouse. Chunking during action sequence learning  
676 was represented with scatter plots of identified sequence elements (see Figures 3G, J, K; Figure 3—  
677 figure supplement 2; Figure 5H; Figure 6H). Action intervals were categorised into within-sequence  
678 IPIs and sequence boundary intervals. Within-sequence IPIs (execution) involved the intervals formed

679 between presses contained within each sequence. Sequence boundary intervals were calculated by  
680 adding up press-check (termination) and check-press (initiation) intervals. Boundary intervals that went  
681 beyond 20 seconds involved engagement in other behaviours and were disregarded. Data in the scatter  
682 plots are random (y axis) and Log10 transformation of element intervals (x axis). Kernel density curves  
683 indicating clustering of each interval type within a particular session are also plotted.

684  
685 **Action data (acoustics).** [Figure 3-source data 3] Due to the temporal bias induced by timestamp-based  
686 data retrieval at short time intervals (see Figure 3—figure supplement 1C), we calculated real inter  
687 press interval times on selected fast sequences on day 18 (see Figure 3A-C). The five fastest sequences  
688 (from the timestamp data) were identified in the video recordings (.asf files) in each mouse, and the  
689 corresponding audio file (.wav) was stripped using VideoLAN software (VLC v2.1.3). Bursts of lever  
690 presses were isolated by identifying the acoustic fingerprint of single lever depressions based on  
691 superimposing the waveform frequency trace (MATLAB) with the matching spectrogram (WaveSurfer  
692 software) (see Figure 3C). This method allowed to confidently distinguishing discrete lever press  
693 sounds over the background noise as well as to rule out lever-bouncing artefacts and other unrelated  
694 sounds. Isolated sequences were confirmed by video inspection. Real IPI and speed data were then  
695 calculated in each burst by measuring the time between and frequency of peaks (see Figure 3C).

696  
697 **Pellet drop detection.** [SourceData 7]. Recordings were performed inside the same mouse operant  
698 conditioning chambers used in all experiments (MED Associates, PO), with all doors closed and the fans  
699 activated. Ten food pellets were randomly delivered to the food receptacle by activating the pellet dispenser  
700 output (electric rotor moves  $1/12^{\text{th}}$  of a turn) with a  $P = 0.1$  each second. Sessions ended when 10 pellets had  
701 been delivered (average session time = 1.66 min). Pellet deliveries were timestamped with 1 ms resolution.  
702 During this time, parallel sound level and vibration recordings were conducted in different devices. Sound level  
703 data was recorded using Sound Analyzer v2.2 at variable time weightings (Fast [F]: 125 ms up and down; Slow

704 [S]: 1 s up and down; and Impulse [I]: 35 ms up and 1.5 s down) and different frequency filters (Z [zero]-filter:  
705 audio range 10 Hz to 20 kHz  $\pm$ 1.5 dB; A-filter: audio range -20 Hz to 20 kHz; C-filter: loud sound detection).  
706 Sound exposure level (E) and equivalent continuous sound level (eq) were also recorded for each filter. Only  
707 recordings best detecting the pellet drop sound are shown in Figure 1—figure supplement 1A. Vibration was  
708 recorded with VibSensor v2.1.1 (Now Instruments and Software) as high-pass filtered accelerometer data (99.3  
709 Hz) on 3 different movement axes (x, y, z).

710

711 ***Phospho-MAPK mapping.*** [Figure 4-source data 1] High-resolution mosaics obtained in Slidebook 6.0  
712 (3 per animal from rostral, medial and caudal sections; see “Image acquisition” section above) were  
713 processed using the non-commercial open-source ImageJ2/Fiji software (v.1.49j10; Wayne Rasband,  
714 National Institutes of Health, USA). The following cortical and striatal regions were analysed:  
715 Prelimbic cortex [PrL], anterior cingulate/Motor region 2 [aCg/M2], anterior dorsal striatum [aDS],  
716 core [Co], shell [Sh], dorsomedial striatum [DMS], dorsolateral striatum [DLS], frontoparietal cortex  
717 [FPx]. The outer boundary of the different cortical and striatal regions was manually drawn in each  
718 hemisection, the area of the region was measured ( $\text{mm}^2$ ), and Cartesian coordinates (x, y) of the points  
719 defining the edge were obtained. To quantify the number of activated neurons and retrieve their  
720 location across the striatum, images were thresholded based on p-MAPK immunolabelling and  
721 individual somata were automatically detected using the “Analyze Particle” command in ImageJ2/Fiji,  
722 which finds the edge of an object, determines its position and outlines its contour creating a region of  
723 interest (ROI). Resulting data, including neuron count, position (x, y coordinates) and area ( $\text{px}^2$ ) of the  
724 centroid of each labeled neuron, was imported into MATLAB (MathWorks, Natick, MA). We then  
725 used a customised script that performs the in-built “inpolygon” function, which returns a list of the  
726 points lying inside the edge of the polygon area (cortical and striatal regions). The spatial distribution  
727 of neurons was digitally reconstructed by combining a line plot defined by the edge points of the  
728 regions and a scatter plot with circles at the locations specified by the neurons’ centroid coordinates.



## 730     **Statistics**

731     Data were analysed using SPSS Statistics software (version 22; IBM Corporation, Somers, NY). The *a*  
732     *priori* alpha level was set at  $p < .05$ . All statistical details of each experiment, including the *n*, the  
733     statistical test applied and significance, can be found in the Results and in the figure and figure legends.  
734     The factors involved are indicated in the text (in brackets). To analyse the effect of one or more  
735     independent variables, Levene's test was first used to test the null hypothesis that the error variance of  
736     each dependent variable was equal across groups, and uni or multi-factorial ANOVA was then  
737     conducted. If one or more repeatedly measured variables were considered, uni- or multifactorial  
738     repeated measures ANOVA was conducted. Homogeneity of variance was tested through Mauchly's  
739     test of sphericity, and Greenhouse-Geisser corrections were considered when sphericity was not met. In  
740     mixed ANOVA analyses involving within-subject and between subjects comparisons, factors in  
741     brackets corresponded to within-subject (first) and between subjects (second). In instances where  
742     further statistical detail was appropriate, we conducted additional simple effects comparisons based on  
743     individual one-way ANOVAs. Statistical comparisons between two means were conducted through  
744     independent t-tests, and equal variances were assumed or not according to the Levene's test for  
745     equality of variances. To measure the relationship between two variables, Pearson's correlation  
746     coefficient (*r*) was calculated, where the value can lie between -1 (as one variable changes, the other  
747     changes proportionally in the opposite direction), to +1 (as one variable changes, the other changes in  
748     the same direction by the same amount). Correlations involved within-subjects measures.

749

## 750     **Acknowledgements**

751     The authors thank Dr Amir Dezfouli and Prof Mark Bouton for insightful discussions, and Dr Richard  
752     Faville and Matthew Van De Poll for assistance in MATLAB programming.

753

## References

- Abrahamse, E.L., Ruitenberg, M.F.L., de Kleine, E., and Verwey, W.B. (2013). Control of automated behaviour: insights from the discrete sequence production task. *Front. Hum. Neurosci.* 7.
- Bailey, M.R., Jensen, G., Taylor, K., Meziar, C., Williamson, C., Silver, R., Simpson, E.H., and Balsam, P.D. (2015). A novel strategy for dissecting goal-directed action and arousal components of motivated behaviour with a progressive hold-down task. *Behav. Neurosci.* 129, 269–280.
- Balleine, B. (2005). Neural bases of food-seeking: Affect, arousal and reward in corticostriatolimbic circuits☆. *Physiol. Behav.* 86, 717–730.
- Balleine, B.W., and O'Doherty, J.P. (2010). Human and rodent homologues in action control: corticostriatal determinants of goal-directed and habitual action. *Neuropsychopharmacology* 35, 48–69.
- Bertran-Gonzalez, J., Håkansson, K., Borgkvist, A., Irinopoulou, T., Brami-Cherrier, K., Usiello, A., Greengard, P., Hervé, D., Girault, J.-A., Valjent, E., et al. (2009). Histone H3 phosphorylation is under the opposite tonic control of dopamine D2 and adenosine A2A receptors in striatopallidal neurons. *Neuropsychopharmacology* 34, 1710–1720.
- Bo, J., Borza, V., and Seidler, R.D. (2009). Age-Related Declines in Visuospatial Working Memory Correlate With Deficits in Explicit Motor Sequence Learning. *J. Neurophysiol.* 102, 2744–2754.
- Cabeza, R., Anderson, N.D., Locantore, J.K., and McIntosh, A.R. (2002). Aging Gracefully: Compensatory Brain Activity in High-Performing Older Adults. *NeuroImage* 17, 1394–1402.
- Dayan, P., and Daw, N.D. (2008). Decision theory, reinforcement learning, and the brain. *Cogn. Affect. Behav. Neurosci.* 8, 429–453.
- Ebrahimi, A., Pochet, R., and Roger, M. (1992). Topographical organization of the projections from physiologically identified areas of the motor cortex to the striatum in the rat. *Neurosci. Res.* 14, 39–60.
- Edin, F., Klingberg, T., Johansson, P., McNab, F., Tegnér, J., and Compte, A. (2009). Mechanism for top-down control of working memory capacity. *Proc. Natl. Acad. Sci.* 106, 6802–6807.
- Fukai, T. (1999). Sequence generation in arbitrary temporal patterns from theta-nested gamma oscillations: a model of the basal ganglia–thalamo-cortical loops. *Neural Netw.* 12, 975–987.
- Garcia-Colera, A., and Semjen, A. (1987). The organization of rapid movement sequences as a function of sequence length. *Acta Psychol. (Amst.)* 66, 237–250.
- Gerfen, C.R., and Surmeier, D.J. (2011). Modulation of Striatal Projection Systems by Dopamine. *Annu. Rev. Neurosci.* 34, 441–466.
- Graybiel, A.M. (1998). The Basal Ganglia and Chunking of Action Repertoires. *Neurobiol. Learn. Mem.* 70, 119–136.
- Gruber, O., and Goschke, T. (2004). Executive control emerging from dynamic interactions between brain systems mediating language, working memory and attentional processes. *Acta Psychol. (Amst.)* 115, 105–121.
- Gunstad, J., Cohen, R.A., Paul, R.H., Luyster, F.S., and Gordon, E. (2006). Age effects in time estimation: relationship to frontal brain morphometry. *J. Integr. Neurosci.* 05, 75–87.



790 Gutchess, A.H., Welsh, R.C., Hedden, T., Bangert, A., Minear, M., Liu, L.L., and Park, D.C. (2005). Aging and  
791 the Neural Correlates of Successful Picture Encoding: Frontal Activations Compensate for Decreased Medial-  
792 Temporal Activity. *J. Cogn. Neurosci.* *17*, 84–96.

793 Hunnicutt, B.J., Jongbloets, B.C., Birdsong, W.T., Gertz, K.J., Zhong, H., and Mao, T. (2016). A comprehensive  
794 excitatory input map of the striatum reveals novel functional organization. *eLife* *5*, e19103.

795 Igarashi, J., Isomura, Y., Arai, K., Harukuni, R., and Fukai, T. (2013). A  $\theta$ – $\gamma$  Oscillation Code for Neuronal  
796 Coordination during Motor Behaviour. *J. Neurosci.* *33*, 18515–18530.

797 Inagaki, N., Igeta, K., Shiraishi, N., Kim, J.F., Nagao, M., Nakamura, N., and Nagai, H. (2003). Evaluation and  
798 characterization of mouse scratching behaviour by a new apparatus, MicroAct. *Skin Pharmacol. Appl. Skin*  
799 *Physiol.* *16*, 165–175.

800 Jin, X., and Costa, R.M. (2010). Start/stop signals emerge in nigrostriatal circuits during sequence learning.  
801 *Nature* *466*, 457–462.

802 Jin, X., and Costa, R.M. (2015). Shaping action sequences in basal ganglia circuits. *Curr. Opin. Neurobiol.* *33*,  
803 188–196.

804 Jin, X., Tecuapetla, F., and Costa, R.M. (2014). Basal ganglia subcircuits distinctively encode the parsing and  
805 concatenation of action sequences. *Nat. Neurosci.* *17*, 423–430.

806 Lashley, K.S. (1951). The problem of serial order in behaviour. In *Cerebral Mechanisms in Behaviour*, (New  
807 York, NY: Wiley), pp. 112–131.

808 Lindenberger, U., and Mayr, U. (2014). Cognitive aging: is there a dark side to environmental support? *Trends*  
809 *Cogn. Sci.* *18*, 7–15.

810 Matamalas, M., Skrbis, Z., Hatch, R.J., Balleine, B.W., Götz, J., and Bertran-Gonzalez, J. (2016a). Aging-  
811 Related Dysfunction of Striatal Cholinergic Interneurons Produces Conflict in Action Selection. *Neuron* *90*,  
812 362–373.

813 Matamalas, M., Götz, J., and Bertran-Gonzalez, J. (2016b). Quantitative Imaging of Cholinergic Interneurons  
814 Reveals a Distinctive Spatial Organization and a Functional Gradient across the Mouse Striatum. *PLOS ONE*  
815 *11*, e0157682.

816 McGeorge, A.J., and Faull, R.L.M. (1989). The organization of the projection from the cerebral cortex to the  
817 striatum in the rat. *Neuroscience* *29*, 503–537.

818 Mello, G.B.M., Soares, S., and Paton, J.J. (2015). A Scalable Population Code for Time in the Striatum. *Curr.*  
819 *Biol.* *25*, 1113–1122.

820 O'Reilly, R.C., and Frank, M.J. (2006). Making working memory work: a computational model of learning in  
821 the prefrontal cortex and basal ganglia. *Neural Comput.* *18*, 283–328.

822 Otto, A.R., Raio, C.M., Chiang, A., Phelps, E.A., and Daw, N.D. (2013). Working-memory capacity protects  
823 model-based learning from stress. *Proc. Natl. Acad. Sci.* *110*, 20941–20946.

824 Park, D.C., and Reuter-Lorenz, P. (2009). The Adaptive Brain: Aging and Neurocognitive Scaffolding. *Annu.*  
825 *Rev. Psychol.* *60*, 173–196.

826 Raz, N. (2005). Regional Brain Changes in Aging Healthy Adults: General Trends, Individual Differences and  
827 Modifiers. *Cereb. Cortex* *15*, 1676–1689.

828 Santos, F.J., Oliveira, R.F., Jin, X., and Costa, R.M. (2015). Corticostriatal dynamics encode the refinement of  
829 specific behavioural variability during skill learning. *eLife* 4, e09423.

830 Schneider, W., and Shiffrin, R.M. (1977). Controlled and automatic human information processing: I. Detection,  
831 search, and attention. *Psychol. Rev.* 84, 1–66.

832 Shea, C.H., Park, J.-H., and Braden, H.W. (2006). Age-related effects in sequential motor learning. *Phys. Ther.*  
833 86, 478–488.

834 Soares, S., Atallah, B.V., and Paton, J.J. (2016). Midbrain dopamine neurons control judgment of time. *Science*  
835 354, 1273–1277.

836 Sternberg, S., Monsell, S., Knoll, R.L., and Wright, C.E. (1978). The Latency and Duration of Rapid Movement  
837 Sequences: Comparisons of Speech and Typewriting. In *Information Processing in Motor Control and Learning*,  
838 (Academic Press), pp. 117–152.

839 Tecuapetla, F., Jin, X., Lima, S.Q., and Costa, R.M. (2016). Complementary Contributions of Striatal Projection  
840 Pathways to Action Initiation and Execution. *Cell* 166, 703–715.

841 Valjent, E., Pagès, C., Hervé, D., Girault, J.-A., and Caboche, J. (2004). Addictive and non-addictive drugs  
842 induce distinct and specific patterns of ERK activation in mouse brain. *Eur. J. Neurosci.* 19, 1826–1836.

843 Valjent, E., Bertran-Gonzalez, J., Aubier, B., Greengard, P., Hervé, D., and Girault, J.-A. (2010). Mechanisms of  
844 Locomotor Sensitization to Drugs of Abuse in a Two-Injection Protocol. *Neuropsychopharmacology* 35, 401–  
845 415.

846 Verwey, W.B. (2010). Diminished motor skill development in elderly: Indications for limited motor chunk use.  
847 *Acta Psychol. (Amst.)* 134, 206–214.

848 Voelcker-Rehage, C. (2008). Motor-skill learning in older adults—a review of studies on age-related differences.  
849 *Eur. Rev. Aging Phys. Act.* 5, 5–16.

850 Voorn, P., Vanderschuren, L.J.M., Groenewegen, H.J., Robbins, T.W., and Pennartz, C.M.. (2004). Putting a  
851 spin on the dorsal–ventral divide of the striatum. *Trends Neurosci.* 27, 468–474.

852 Wang, M., Gamo, N.J., Yang, Y., Jin, L.E., Wang, X.-J., Laubach, M., Mazer, J.A., Lee, D., and Arnsten, A.F.T.  
853 (2011). Neuronal basis of age-related working memory decline. *Nature* 476, 210–213.

854 Wingfield, A., Stine, E.A.L., Lahar, C.J., and Aberdeen, J.S. (1988). Does the capacity of working memory  
855 change with age? *Exp. Aging Res.* 14, 103–107.

856 Wymbs, N.F., Bassett, D.S., Mucha, P.J., Porter, M.A., and Grafton, S.T. (2012). Differential Recruitment of the  
857 Sensorimotor Putamen and Frontoparietal Cortex during Motor Chunking in Humans. *Neuron* 74, 936–946.

858 Yin, H.H., Mulcare, S.P., Hilário, M.R.F., Clouse, E., Holloway, T., Davis, M.I., Hansson, A.C., Lovinger,  
859 D.M., and Costa, R.M. (2009). Dynamic reorganization of striatal circuits during the acquisition and  
860 consolidation of a skill. *Nat. Neurosci.* 12, 333–341.

861

## Figures, Figure supplements and Videos

### Figure 1.

**Evidence of sequence learning in aged mice.** [Figure 1-source data 1] (A) Experimental design of instrumental conditioning under an increasing random ratio (RR) schedule of reinforcement, from constant reinforcement (CRF) to RR20. Sequence triggering (ST) programs were introduced on day 10. (B) Initiation, execution and termination elements were identified in each sequence according to lever press (LP) and magazine entry interspersing. (C) Number of action sequences per minute (sequence rate) displayed throughout instrumental learning [StatsReport1]. (D, E) Average length (D) and duration (E) of LP sequences produced by each young and aged mouse on days 7 and 17 of training. Orange traces represent individual mice. Asterisks denote significant day x age interaction (red) and simple effects (black, see text). N.S., not significant [StatsReport2] [StatsReport3]. (F) Event-time diagrams showing linearly organised LP sequences produced by all young and aged mice on training day 17. Shaded segments (gray) are amplified LP sequences (seconds). See Figure 1—figure supplement 1D for pre-sequence diagrams.

### Figure 1—figure supplement 1.

**Application of a sequence trigger (ST) to promote sequence learning.** [Figure 1-source data 1] (A) ST (applied from day 10 onwards) limited the access to RR reinforcement to action sequences that were initiated with at least 5 (from day 10) or 7 (from day 13) consecutive lever presses. Sequences that were truncated with a termination element (lever press → magazine entry) before reaching the fifth or seventh consecutive press blocked access to the RR program. Unlocked sequences ( $\geq 5$  initial presses) that were truncated with a termination element before earning reward (+n presses) also reset the RR trial. (B) Overall LP rate during acquisition of instrumental behaviour (presses/min) [StatsReport25]. (C) Number of sequences that went through ST5. Only days where ST was applied are plotted (days 10-17). Asterisk denotes significant training x age interaction [StatsReport26]. (D) Event-time diagrams showing linearly organised LP sequences produced by all young and aged mice on training day 7 (pre-sequence). See Figure 1F for post-sequence diagrams.

### Figure 1—figure supplement 2.

**Pellet drop detection in operant conditioning chambers.** [Figure 1-source data 2] [Figure 1-source data 3] (A) Simultaneous recording of sound level (top traces), vibration (middle trace) and pellet dispenser rotor activation (bottom trace) during random delivery of 10 pellets across 1.5 min. Sound level (L) is shown at two different frequency weightings (yellow trace: Z [zero]-filter, 10 Hz to 20 kHz; red trace: A-filter, -20 Hz to 20 kHz) with fast time weighting (F: 125 ms). Vibration was based on high-pass filtered accelerometer data (99.3 Hz) on 3 different movement axes (x, y, z). Pellets were randomly delivered through activation of an electric rotor (1/12<sup>th</sup> of a turn) on a dispenser located outside of the chamber. (B, C) [StatsReport23] [StatsReport24] Average first-check intervals (B) and magazine check rate (C) across 6 sessions of magazine training. Twenty pellets were delivered randomly over an average 30 min period. (D) Representation of each individual pellet delivery → magazine check intervals displayed by all young and all aged mice on the first and the last day of magazine training. Emergence of red squares (overlay) denotes close pellet delivery and magazine check times. Pellet delivery → magazine check pairs are distributed randomly in the y axis.

### Figure 2.

907  
908  
909  
910  
911  
912  
913  
914  
915  
916  
917  
918  
919  
920  
921  
922  
923  
924  
925  
926  
927  
928  
929  
930  
931  
932  
933  
934  
935  
936  
937  
938  
939  
940  
941  
942  
943  
944  
945  
946  
947  
948  
949  
950

**Aged mice are unable to temporally sustain their actions.** [Figure 2-source data 1] [StatsReport4] (A) Mice were trained to press and hold the lever down for increasing periods to obtain rewards. (B) Experimental design of instrumental conditioning under an increasing pseudorandom lever hold (LH) schedule of reinforcement. Average LH times are indicated in seconds. (C) Acquisition of LH instrumental behaviour across training. Data are mean  $\pm$  SEM (7 and 8 mice per group). Asterisk denotes significant training  $\times$  age interaction. (D) Representation of each individual LH performed by all young and all aged mice on the last day of LH0.3, LH0.8, LH2, LH3.2 and LH5 training. LH times are presented in a Log10 scale (x axis), and sequences are distributed randomly in the y axis.

**Figure 2—figure supplement 1.**

**Aged mice produce shorter lever holds.** [Figure 2-source data 1] Timestamp diagrams showing linearly organised LH sequences produced by each young and aged mouse (Subjects #1 to #8 and #1 to #7) during the first 100 seconds of the last day of LH5 training (day 17). LH time (grey shade) is flanked by lever down (blue segment, initiation) and lever up (green segment, termination) timestamps.

**Figure 3.**

**Aged mice produce ultrafast sequences and aberrant chunking.** [Figure 1-source data 1] [Figure 3-source data 3] (A) Average sequence speed calculated from timestamp data after 20 minutes of continuous instrumental performance on training day 18 [StatsReport33]. (B) Frequency distribution of the number of inter-press-intervals (IPIs) recorded in all young and aged mice at increasing intervals on training day 18. (C) Real IPIs from the fastest sequence recorded in a young and an aged mouse on day 18 (Fast sequence 1 in Video 1 and Video 2). Real lever press times were identified by aligning the sound waveform (top) and acoustic spectrogram (bottom) generated by lever press activity during the session. Identified presses are marked with a blue dashed line. (D, E) Average speed (B) and IPIs (C) of the 5 fastest LP sequences displayed by young and aged mice during the 20-min session on day 18 extracted from acoustic data [StatsReport5] [StatsReport6]. (F) Efficiency of LP instrumental behaviour (rewards earned per minute) in young and aged mice on day 18 [StatsReport7]. Asterisks (B-D) denote significant effects (see text). (G) Scatter plots of each within-sequence inter-press-interval (IPIs, blue) and sequence boundary interval (orange) produced by one young and one aged mouse (Young #7 and Aged #5) at different stages of training. Kernel density curves of each interval type are plotted at the bottom. Grey shades delimitate the within-sequence chunking space. (H, I) Average within-sequence IPIs (G) and sequence boundary (H) intervals. Insets are corresponding standard deviations. Data are mean  $\pm$  SEM. Asterisk denotes significant training  $\times$  age interaction [StatsReport27] [StatsReport28] [StatsReport31] [StatsReport32]. (J, K) Proportional scatter plots and kernel density curves showing intervals of the within-sequence (I) and sequence boundary (J) elements produced by all young and all aged mice during the first 600 seconds of training day 18. Insets are the total element counts for this period [StatsReport29] [StatsReport30]. Data in A, D-F, J and K are mean  $\pm$  SEM. *p*, *p*-value; asterisk, significant effect; N.S., not significant.

**Video 1. Representative performance of a young mouse during the last day of sequence training.** Two fast action sequences are captured (indicated in red font, top left corner). Fast action sequence 1 is represented in Figure 3A. Subject Young#5; active lever: right; training day 18.

**Video 2. Representative performance of an aged mouse during the last day of sequence training.** Two fast action sequences are captured (indicated in red font, top right corner). Fast action sequence 1 is represented in Figure 3A. Subject Aged#4; active lever: left; training day 18.

**Figure 3—figure supplement 1.**

**Ultra-fast IPIs in aged mice.** [Figure 1-source data 1] [StatsReport8] **(A)** Quantification of the number of IPIs under 2.5 seconds, 200 msec and 150 msec in young and aged mice on day 18. Data are mean + SEM. N.S, not significant ( $\leq 2.5$  sec:  $t_{(14)} = 0.799$ ,  $p = 0.438$ ). Asterisks denote significant difference ( $< 200$  msec:  $t_{(14)} = -2.564$ ,  $p < 0.05$ ;  $< 150$  msec:  $t_{(8,492)} = -2.898$ ,  $p < 0.05$ ). **(B)** Representation of all IPIs produced by all young and aged mice on training day 18 (RAND, random). Note that the 10 msec-based timestamp generated placement artefacts in IPIs under 100 msec. Intervals of 20 to 90 msec are biologically improbable (red asterisks). Real-time IPIs were therefore studied through acoustics analysis (see Figure 3C-E).

**Figure 3—figure supplement 2.**

**Sequence boundary intervals in aged mice are regularised early in training.** Scatter plots of within-sequence inter-press-intervals (IPIs, blue) and sequence boundary intervals (orange) produced by each young **(A)** and each aged **(B)** mouse on training day 10. Kernel density curves of each interval type are plotted at the bottom. Graphs Young#7 and Aged#5 are shown in Figure 3G.

**Figure 4.**

**Action sequence features correlate with defective activation of caudolateral corticostriatal networks in aged mice.** [Figure 4-source data 1] **(A)** Extensive analysis of neuronal activation in different rostrocaudal cortical (prelimbic [PrL], anterior cingulate/motor area 2 [aCg/M2], frontoparietal [FPx]) and striatal (anterodorsal [aDS], core, shell, dorsomedial [DMS], dorsolateral [DLS]) areas after 20 minutes of uninterrupted instrumental performance (day 18). **(B)** Position and intensity of each activated neuron (p-Thr<sub>202</sub>-Tyr<sub>204</sub>-MAPK-immunoreactive [p-MAPK]) were detected through semi-automated quantitative fluorescence (~60,000 neurons analysed). **(C)** Horizontal floating bar chart displaying the quantification of p-MAPK counts in different cortical and striatal areas of young and aged mice. Minimum, maximum and mean of the data are represented (vertical lines). Circles indicate individual counts for each animal (8 mice per group). Asterisks denote significant age x region interaction (red) and simple effects (black, see text) [StatsReport9]. **(D)** Activity – performance correlation study comparing the counts of p-MAPK detected in the different cortical and striatal areas (arranged from rostro-medial to caudolateral) and the action sequence features (length, duration and speed) as well as overall instrumental performance (total number of lever presses) displayed by each young and aged mouse during the last day of training. The corresponding  $p$  value matrix (bottom inset) indicates the significance of each correlation. Pearson  $r$  (multicolor scale) and  $p$  (green scale) value diagrams are shown for each correlation [StatsReport10]. **(E)** Cross-correlation analysis of the p-MAPK activity recorded in the different areas (arranged from rostromedial to caudolateral) in all young (left) and aged (right) mice. Multi-colored diagrams show the extent of correlation between each pair of regions (Pearson  $r$  values), and green diagrams (right) indicate their significance at each position ( $p$  values) [StatsReport11]. Correlations in D and E involve within-subjects measures. **(F)** Digitised reconstructions of the distribution of activated neurons in corticostriatal regions at rostral (left), medial (middle) and caudal (right) levels in one young and one aged mouse. Each dot represents the position of one neuron expressing p-MAPK.

**Figure 5.**

**Chemogenetic inhibition of dorsolateral direct pathway neurons increases within-sequence speed.** [Figure 5-source data 1] A cohort of 7 *Drd1a*-Cre<sup>(-)</sup>:*Drd2*-eGFP and 7 *Drd1a*-Cre<sup>(+)</sup>:*Drd2*-eGFP young mice (dSPN-hM4Di<sup>(-)</sup> and dSPN-hM4Di<sup>(+)</sup>) were bilaterally injected with AAV2-hSyn-DIO-hM4Di-mCherry in the DLS. (A) Diagram shows the overlapping spread of viral infection in all dSPN-hM4Di<sup>(+)</sup> mice throughout the DLS as visualised by mCherry-expressing territories. Blue dots represent mapped p-MAPK-positive neurons in the same sections. (B) Upon recovery, all mice were submitted to LP sequence training with daily CNO injections from day 10 (3 mg/kg, 45 min before each session). (C) Number of action sequences per minute (sequence rate) displayed throughout instrumental learning. Data are mean ± SEM. Asterisk denotes significant between subjects effect across CNO period (see text) [StatsReport37]. (D, E) Average length (D) and duration (E) of LP sequences produced by each mouse on days 10 and 17 of training. Orange traces represent individual mice. Asterisks denote significant day x group interaction (red) and simple effects (black, see text) [StatsReport13] [StatsReport14]. (F) Average speed of the LP sequences displayed by dSPN-hM4Di<sup>(-)</sup> and dSPN-hM4Di<sup>(+)</sup> on day 18 (timestamp data) [StatsReport15]. (G) Frequency distribution of the number of inter-press-intervals (IPIs) recorded in all dSPN-hM4Di<sup>(-)</sup> and dSPN-hM4Di<sup>(+)</sup> mice at increasing intervals on training day 18. (H, I) Scatter plots and kernel density curves showing intervals of the within-sequence (H) and sequence boundary (I) elements produced by all dSPN-hM4Di<sup>(-)</sup> and dSPN-hM4Di<sup>(+)</sup> on training day 18. Insets are the total element counts for this period [StatsReport35]. (J, K) Average within-sequence IPIs (J) and sequence boundary (K) intervals on day 18. Data are mean + SEM [StatsReport16] [StatsReport36]. (L) Efficiency of LP instrumental behaviour (rewards earned per minute) in by dSPN-hM4Di<sup>(-)</sup> and dSPN-hM4Di<sup>(+)</sup> mice on day 18 [StatsReport17]. Asterisks denote significant effects (see text). N.S., not significant.

**Figure 5—figure supplement 1.**

**Specific inhibition of dSPN activity in the DLS through chemogenetics.** [Figure 5-source data 2] [Figure 5-source data 1] (A) Young *Drd1a*-Cre:*Drd2*-eGFP double transgenic mice were unilaterally microinjected with AAV2-hSyn-DIO-hM4Di-mCherry (1ul/injection) in a vast extension of the dorsolateral striatum. (B) Upon recovery, the mice were administered with CNO (3 mg/kg, i.p., t=0), challenged with GBR (15 mg/kg, i.p., t=30) and perfused at t=45 minutes. (C) Confocal micrographs showing the extent of viral infection in the DLS three weeks after surgery. (D) High magnification confocal micrographs showing the specificity of dSPN infection and the efficiency of the chemogenetic inhibition through simultaneous detection of eGFP (iSPNs), the viral infection reporter mCherry (dSPNs) and the neuronal activity marker (p-MAPK) in infected vs. control (noninfected) hemispheres of the same mouse. (E) Quantification of p-MAPK density in infected (ipsilateral to injection) and control (contralateral to injection) areas of the DLS. Inset shows the mean areas of the regions of interest quantified. Data are mean + SEM. Asterisk denotes significant paired effect. N.S., not significant [StatsReport34]. (F) Overall performance (LP rate) of bilaterally injected dSPN-hM4Di<sup>(-)</sup> and dSPN-hM4Di<sup>(+)</sup> mice before and after CNO treatment. Data are mean ± SEM [StatsReport12].

**Figure 5—figure supplement 2.**

**Development of action sequences in dSPN-hM4Di(-) and dSPN-hM4Di(+) mice.** [Figure 5-source data 1] (A, B) Event-time diagrams showing linearly organised LP sequences produced by all dSPN-hM4Di(-) and all

dSPN-hM4Di(+) littermates on training day 17. A period of 150 seconds in which all animals performed action sequences was chosen.

## Figure 6.

**Cues signalling sequence termination temporarily normalise action structure in aged mice.** [Figure 6-source data 1] (A) Aged mice were submitted to extended LP sequence training where the termination element in each sequence was cued with a 0.75s white noise. One group maintained the termination cue until training day 36 (Cue Maintained), whereas in the other group (Cue Lost) the cue was removed from day 19. (B) Resulting acquisition of LP instrumental behaviour. Data are mean  $\pm$  SEM (6-8 mice per group). Asterisk denotes significant overall effect of training (see text) [StatsReport18]. (C, D) Average length (C) and duration (D) of the LP sequences produced by both groups on days 7, 18 and 19 of training. Asterisks denote significant day  $\times$  group interaction (red) and simple effects (black, see text). N.S., not significant [StatsReport19] [StatsReport20]. (E) Structure of LP sequences produced by a “Cue Maintained” and a “Cue Lost” mouse at the start and at the end of the session on training day 19. See also Figure 6—figure supplement 1. (F) Average length of the 10 first sequences and the 10 last sequences produced by “Cue Lost” mice on training day 19. Asterisks denote significant sequence  $\times$  start/end period interaction (red) and simple effects (black, see text). N.S., not significant [StatsReport21]. (G) Total number of action sequences produced in each day of training before and after the loss of the termination cue. Asterisks denote significant overall effect of training (black) and training  $\times$  group interaction (red, see text) [StatsReport22]. (H) Scatter plots of each within-sequence inter-press-interval (IPIs, blue) and sequence boundary interval (orange) produced by one “Cue Maintained” (subject #R8\_M) and one “Cue Lost” (subject #B4\_L) mouse across different days of training. Kernel density curves of each interval type are plotted at the bottom. Grey shades delimitate the within-sequence chunking space.

## Figure 6—figure supplement 1.

**Aged mice lose action structure as soon as feedback cues are removed.** [Figure 6-source data 1] Aged mice underwent LP sequence training with cued termination elements (see Figure 6A). (A, B) Structure of LP sequences produced by all “Cue Maintained” (A) and all “Cue Lost” (B) mice at the session start and at the session end of training day 19. Subjects “Cue Maintained” #3 and “Cue Lost” #8 are shown in Figure 6H.

## Supplementary material

Figure 1-source data 1. Source data for Figures 1 and 3.

Figure 1-source data 2.

Figure 1-source data 3.

Figure 2-source data 1.

Figure 3-source data 1.

Figure 4-source data 1.

Figure 5-source data 1.

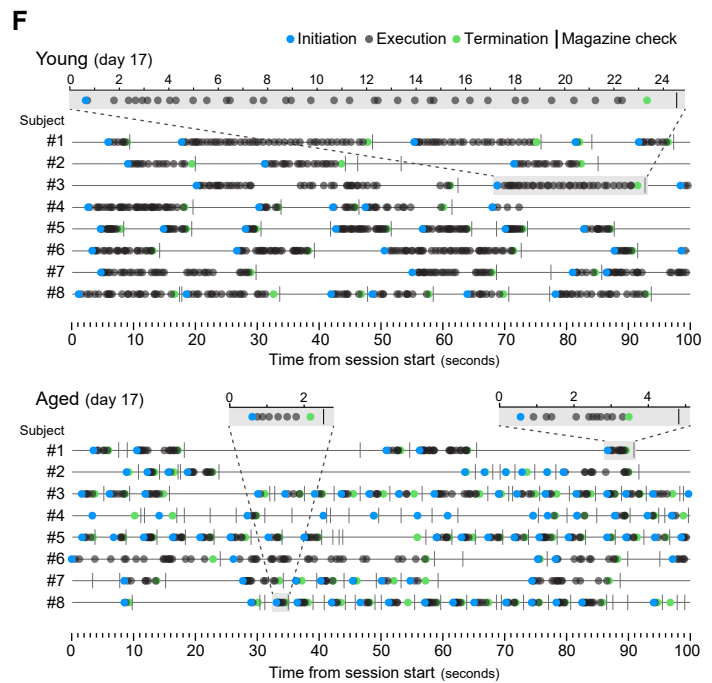
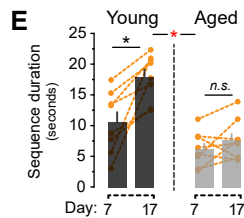
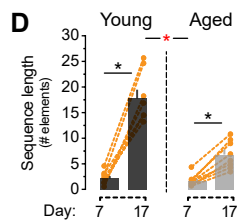
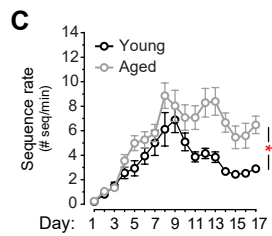
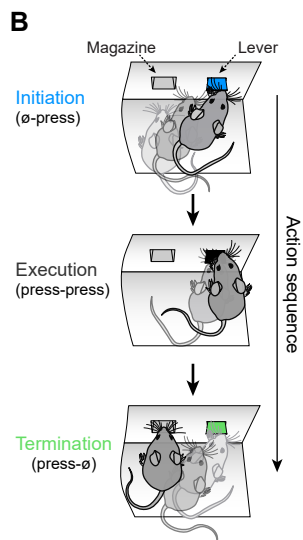
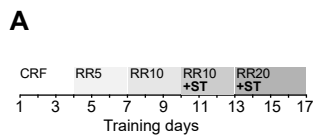
Figure 5-source data 2.

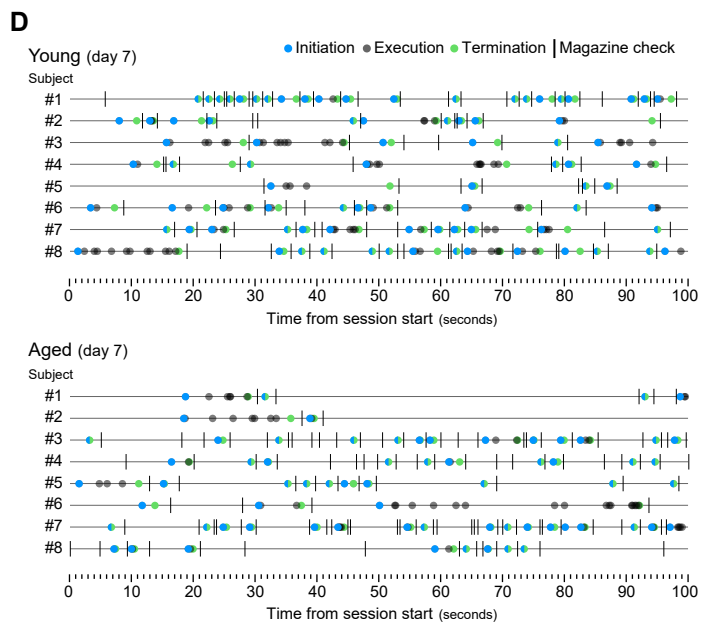
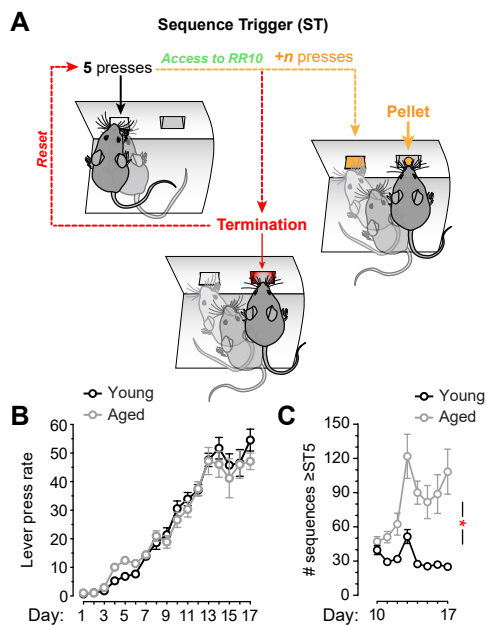
Figure 6-source data 1.

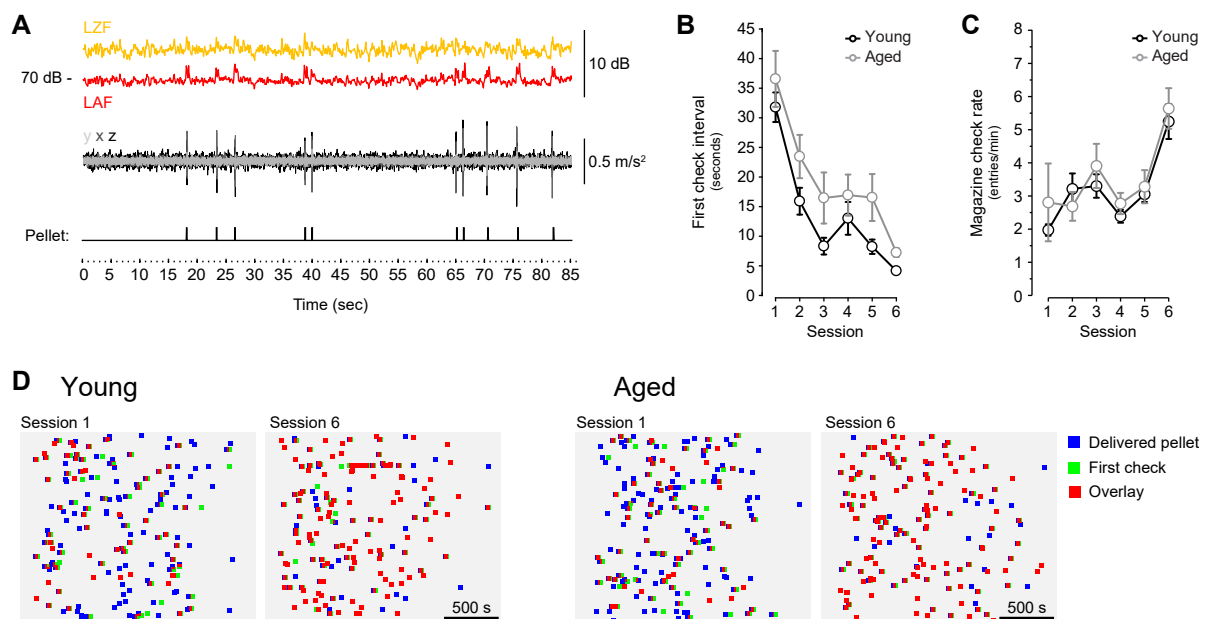
1088

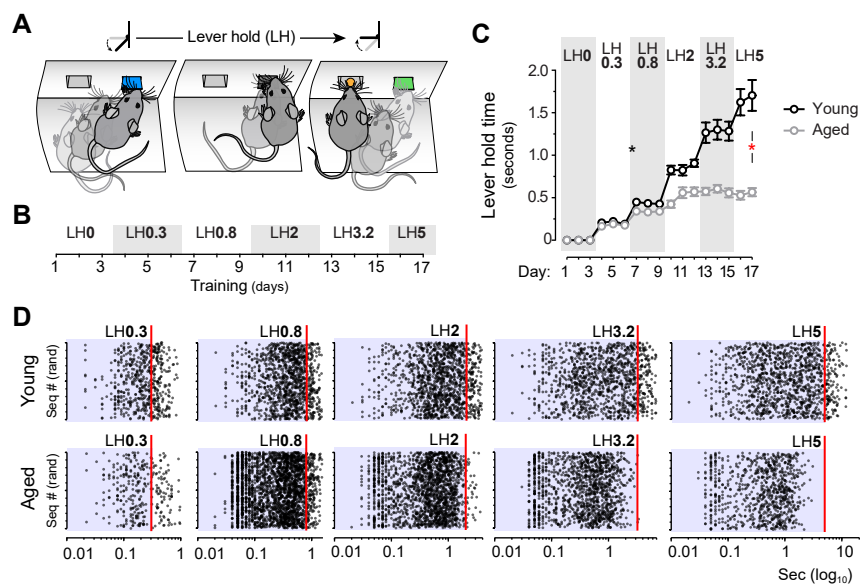
1089 **Supplementary File 1. Stats reports.**

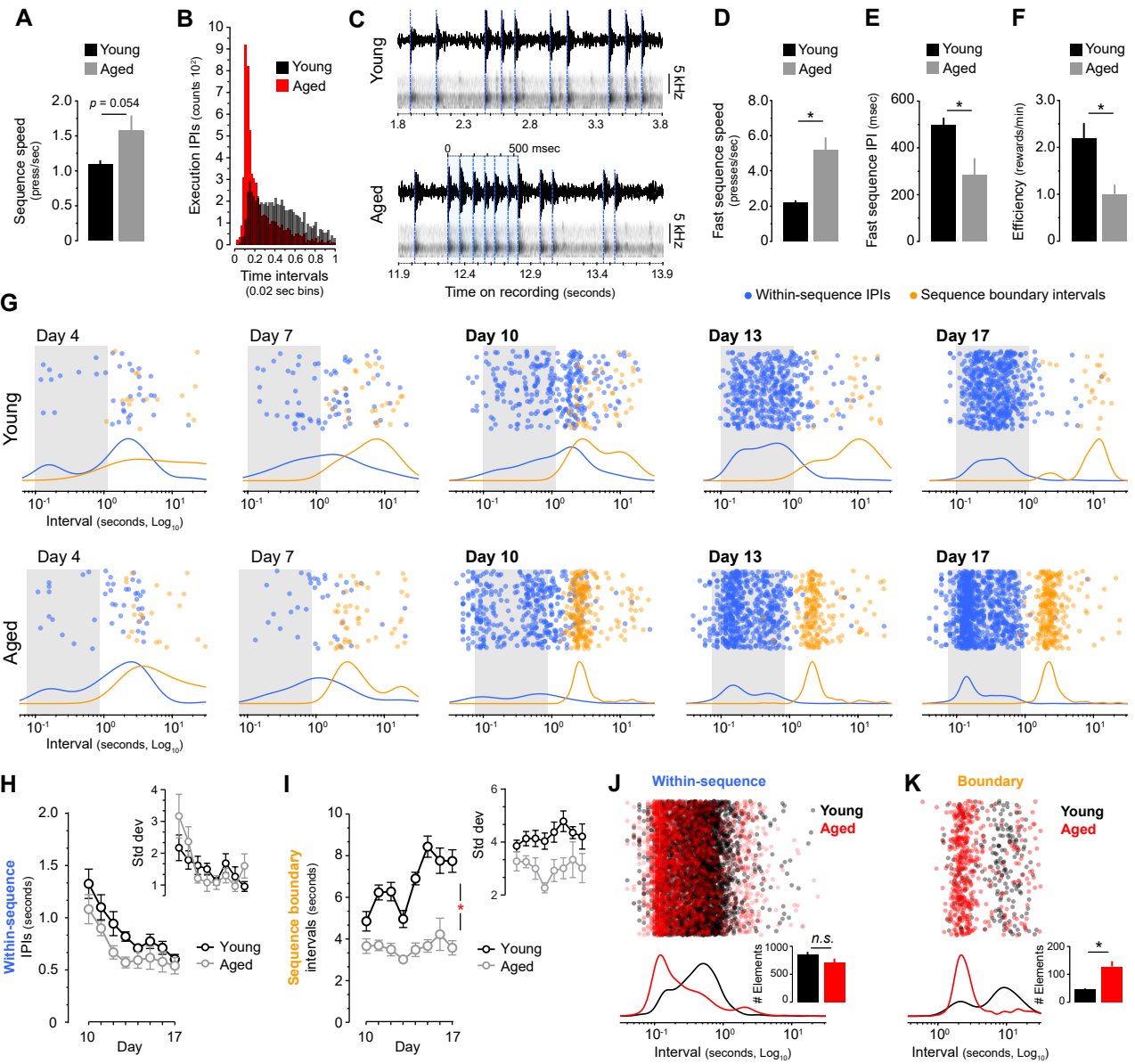


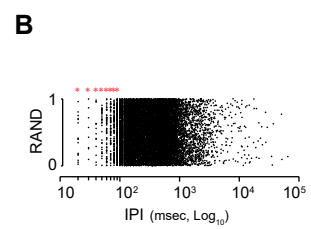
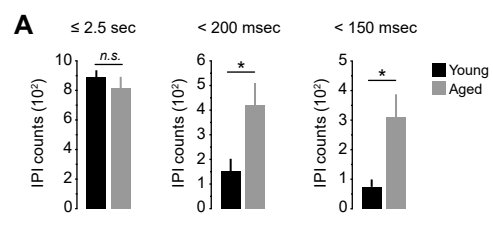




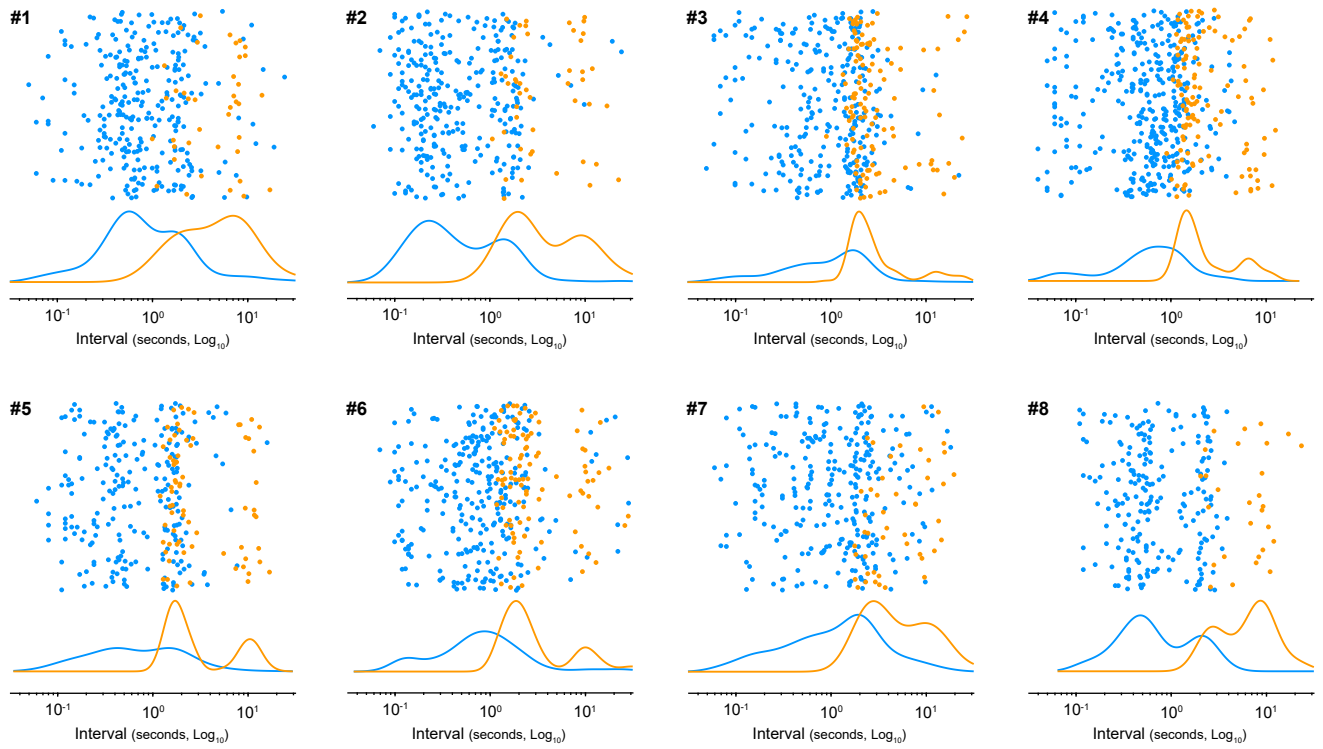




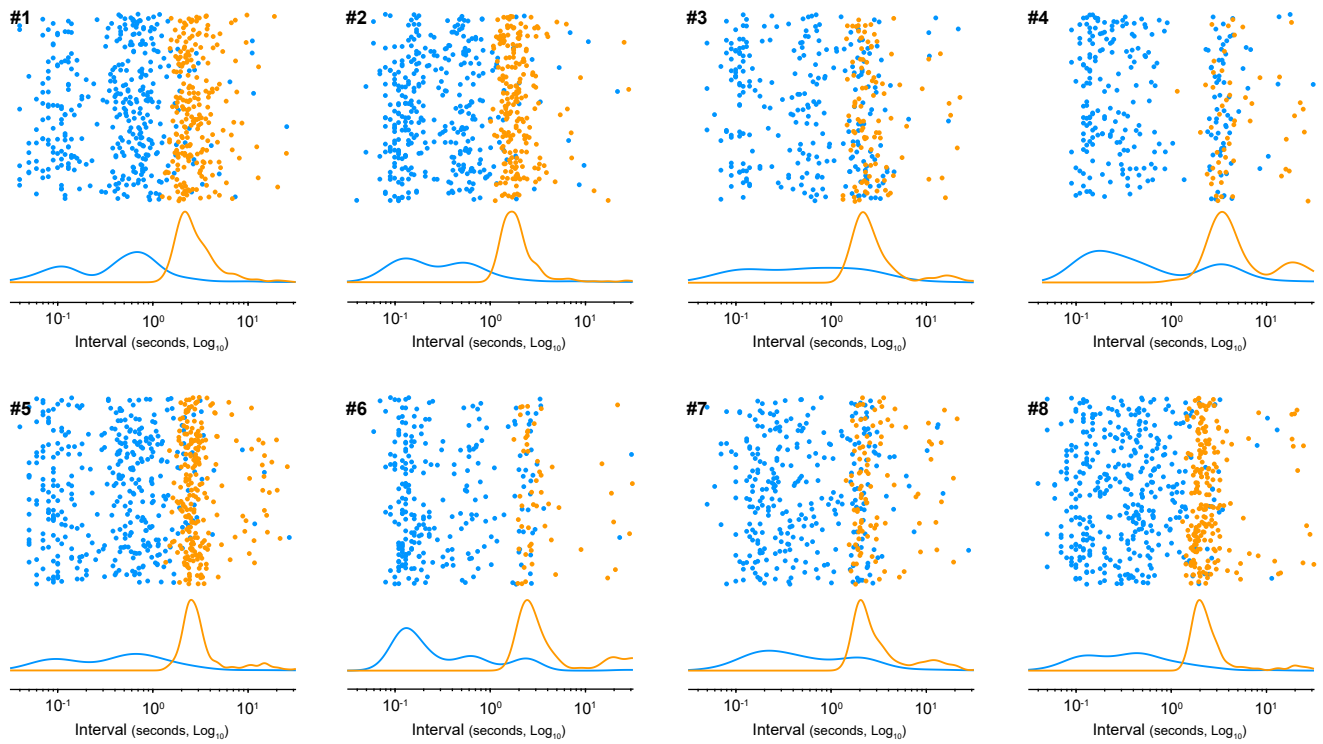


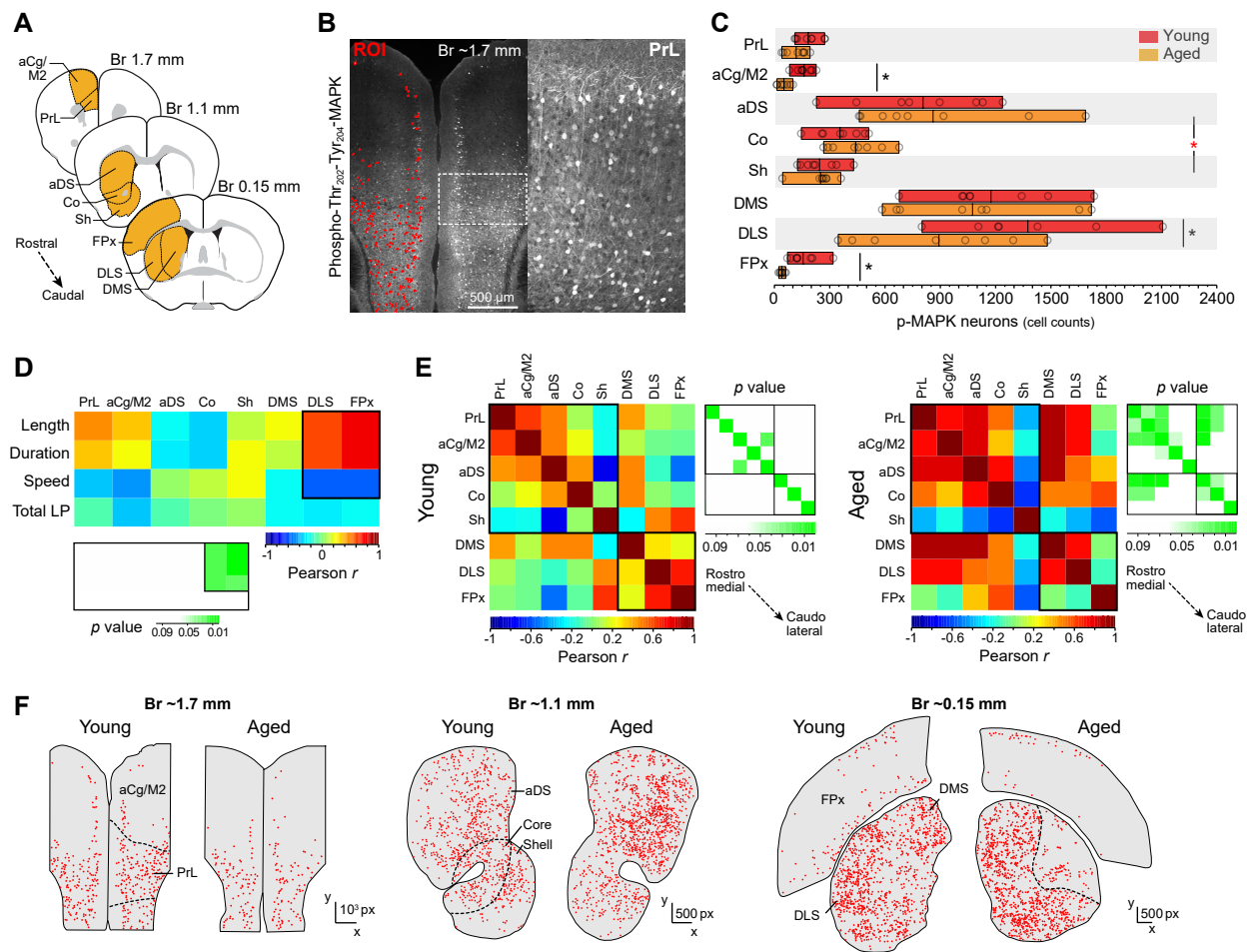


## A Young (day 10)

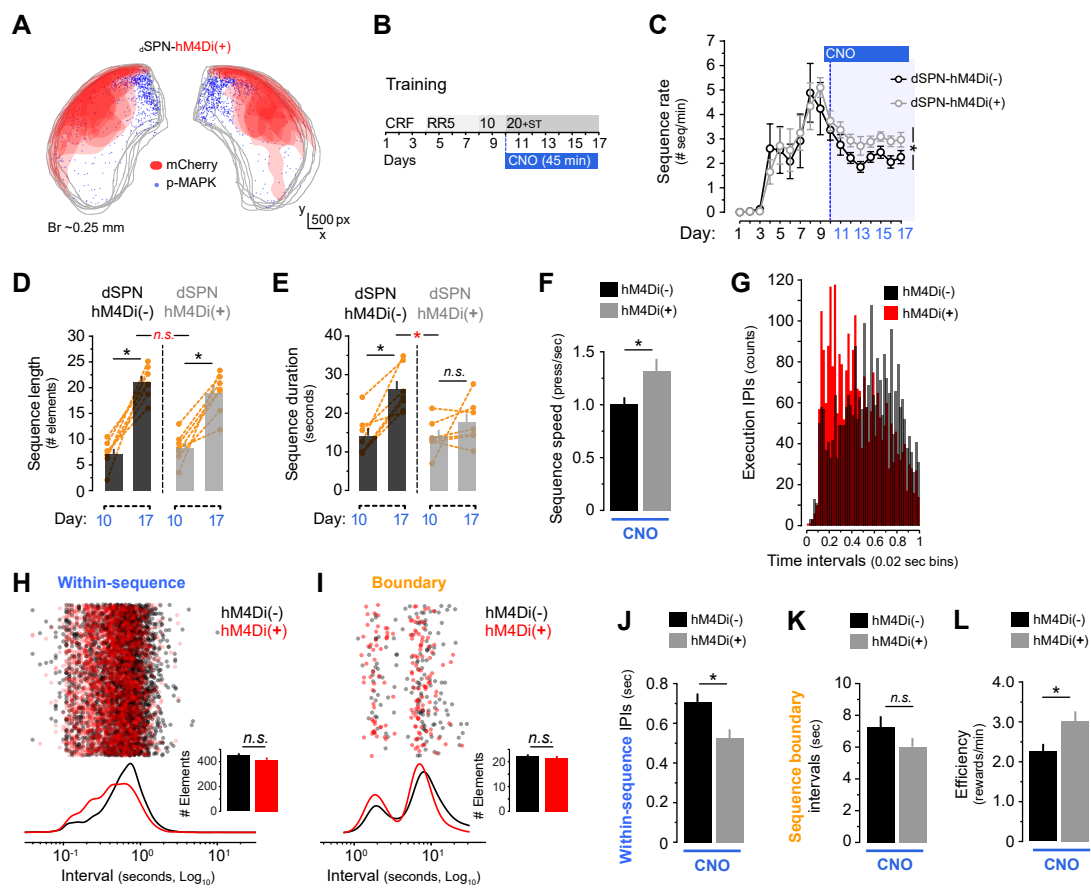


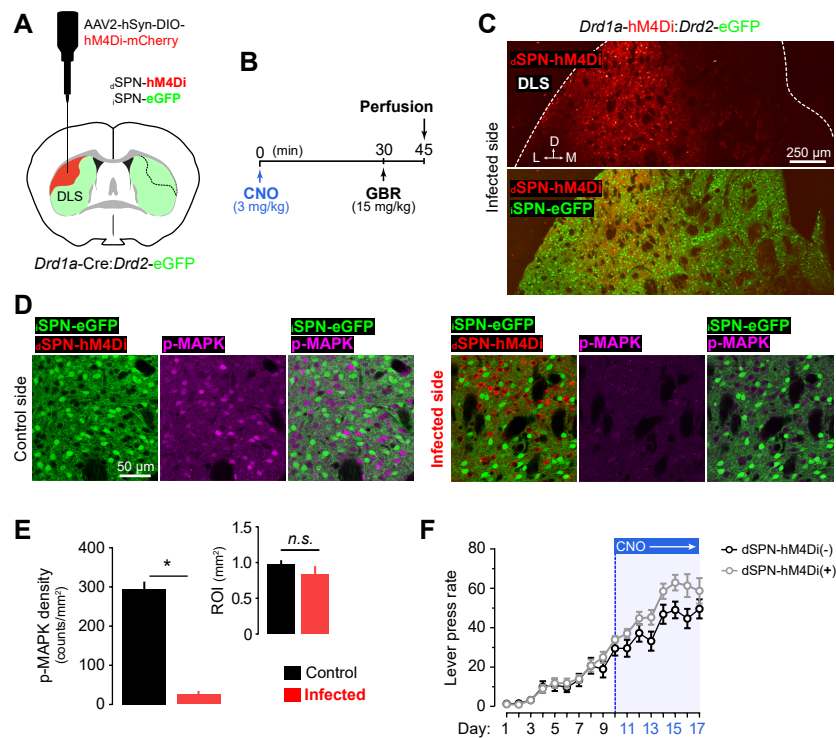
## B Aged (day 10)



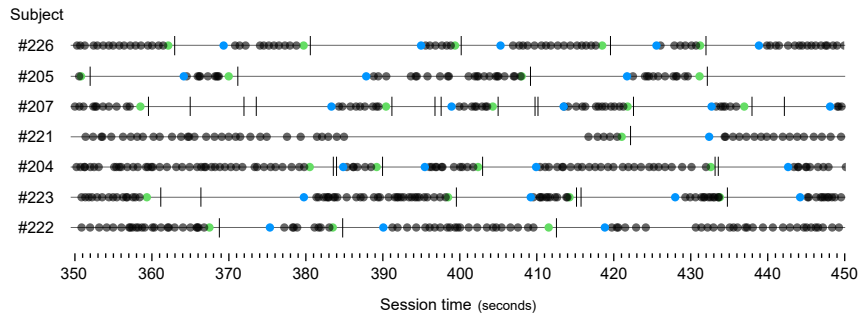




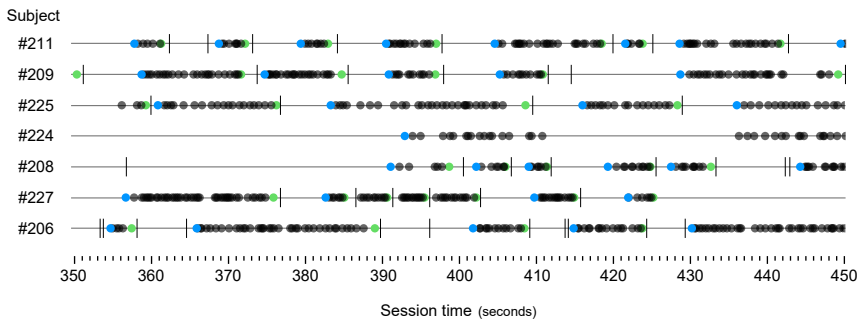


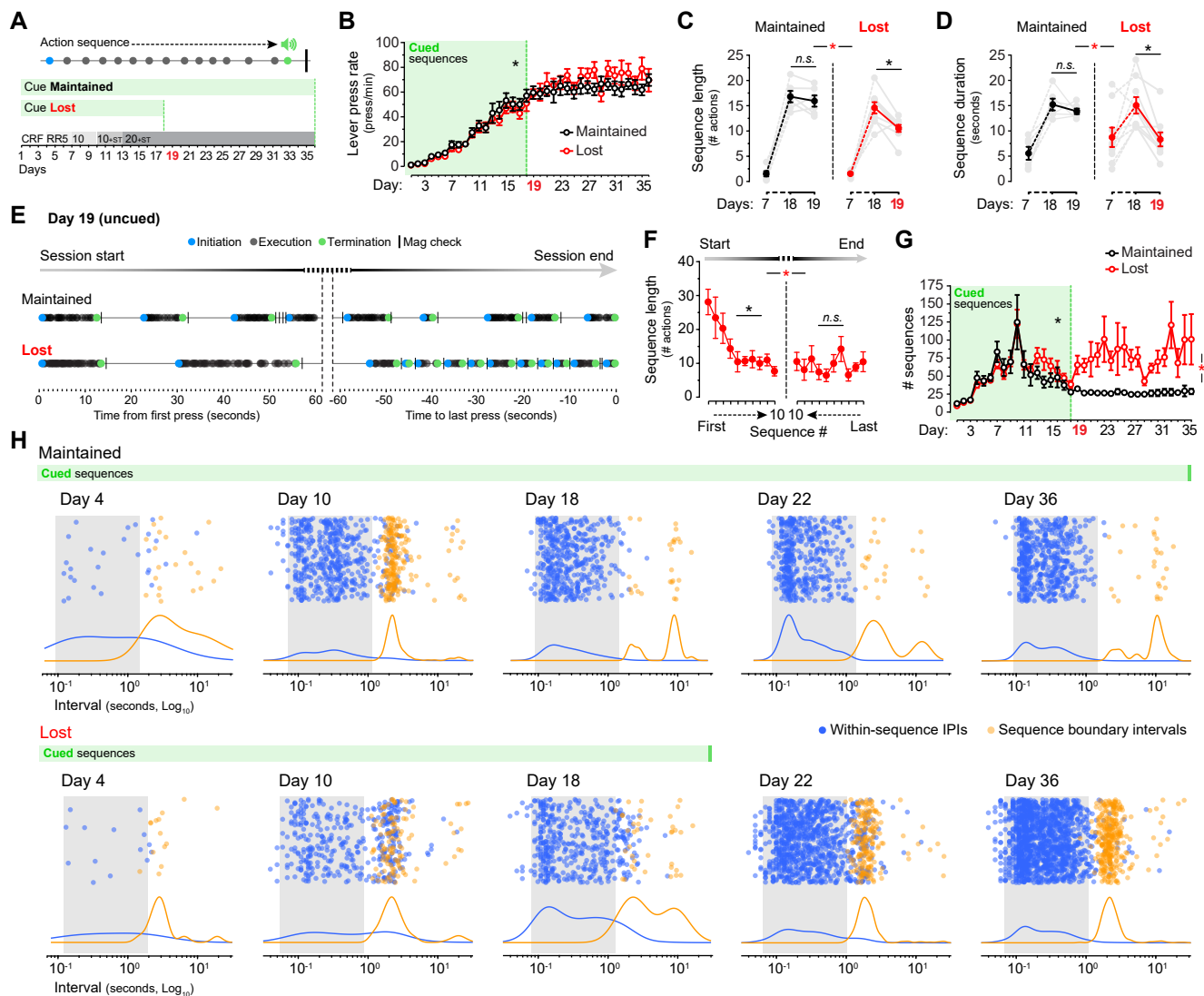


**A** dSPN-hM4Di(-) (day 17)

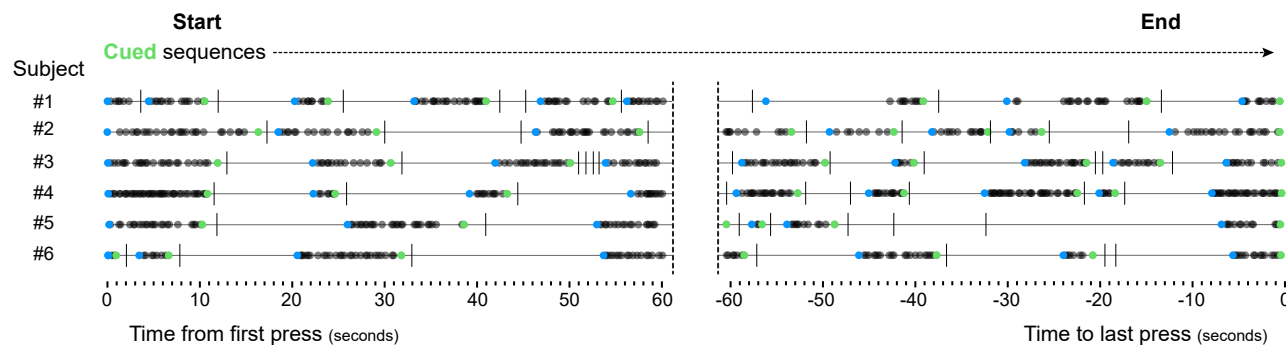


**B** dSPN-hM4Di(+) (day 17)





## A Cue Maintained



## B Cue Lost

